Genetically Engineered Solid Binding Peptides (GEPI) for Surface Biofunctionalization Applications: Immobilization of Enzymes and Antimicrobial Peptides on Solids

Deniz Tanil Yucesoy

A thesis

submitted in partial fulfillment of the

requirements for the degree of

Master of Science

University of Washington

2014

Committee:

Candan Tamerler

Peter Pauzauskie

Mehmet Sarikaya

Program Authorized to Offer Degree:

Department of Materials Science and Engineering

University of Washington

Abstract

Genetically Engineered Solid Binding Peptides (GEPI) for Surface Biofunctionalization Applications: Immobilization of Enzymes and Antimicrobial Peptides on Solids

Deniz Tanil Yucesoy

Chair of the Supervisory Committee:

Professor Candan Tamerler

Materials Science and Engineering

Biological activation and functionalization of solid material interfaces by functional integration of biomolecules is emerging as one of the most dynamic fields of research, impacting a diverse array of applications. Recent advances in translating the biomolecular mechanisms into the hybrid materials and systems design promise novel methodologies that may transform some of our engineering approaches. One of the key issues on design of such systems is the integration of bioactive molecules at the material interfaces without compromising their spatial distribution, surface organization and orientation-dependent bioactivity within a desired proximity. Here, we propose to demonstrate the effective utilization of specific solid binding peptides as anchoring molecules that can be further functionalized to create chimeric peptides. These chimeric molecules are engineered to have built-in solid binding surface binding property in addition to displayed biological functionality as shown by two different case studies.

In case study I, we take the initial steps toward designing multifunctional, enzyme-based platforms by genetically integrating the engineered solid binding peptide tags for tethering redox enzymes onto electrode surfaces. Specifically, utilizing the gold binding peptide (AuBP2) as a molecular erector, we engineered a fusion protein that genetically conjugates to the formate dehydrogenase (FDH) enzyme. Following the binding kinetics and catalytic activity analysis of fusion protein, we created a circuit-based biosensor system and demonstrated the effectiveness of the fusion FDH enzyme electrode over multiple cycles by addition of formate as the substrate.

In case study IIA and IIB, the capability of GEPI's on biomolecular surface functionalization was demonstrated. Here, titanium alloy and zirconium implant surfaces were coated with implant binding peptides which were conjugated to another peptide domain which was engineered with antimicrobial property, resulting a chimeric peptide compromising both solid binding (GEPI's) and antimicrobial (AMP) properties. The efficiency of chimeric/bifunctional peptides both in solution and on titanium surface was evaluated *in vitro* against common oral and orthopedic infectious organisms, *S. mutans* and *S. epidermidis*, respectively and a control organism *E. coli*.

Our findings demonstrate the successful utilization of solid binding peptides as anchoring molecules to design engineered peptide-mediated self-integrated electrode systems and medical devices. The molecular recognition based self-organization of solid binding peptides can be extended to develop a wide range of application where they can be part of biosensing, energy harvesting, biomedical platforms build upon their utilization as biological building blocks combining different combinations of solid materials to large repertoire of biomolecules.

Table of Contents

LIST OF FIGURES

LIST OF TABLES

ACKNOWLEDGEMENTS

I am grateful to all those that helped me with this project and made it a success. I owe my deepest gratitude to Professor Candan Tamerler for being an excellent research advisor and for providing insight and guidance throughout my graduate studies.

I would like to give a huge thank to Professor Mehmet Sarikaya for guiding me to the completion of my thesis and his incites to these projects.

I would like to thank the members of my master's supervisory committee: Professors Candan Tamerler, Mehmet Sarikaya and Peter Pauzauskie for their support and guidance.

I am grateful to my colleagues Dr. Marketa Hnilova, Dr. Sefa Dag, Dr. Hanson Fong, Dr. Mustafa Gungormus and Carolyn Gresswell for their help. I appreciated all their advice and guidance that they have given me over the years as both coworkers and as friends.

1. Introduction- Challenges of immobilization of biological agents on inorganic solid surfaces

The functional integration of biomolecules to the nanostructured materials is emerging as one of the most dynamic field of research, bringing the many areas of engineering and science together.[1] The effective combination of biology into those diverse areas of engineering and science offers an incredible potential to yield a revolutionary advances in bio-nanotechnology and also promises to develop novel devices and systems that enable multiplexed medical diagnosis, environmental sampling, energy harvesting, and data storage. However, there are many challenges to design such bio-hybrid materials that may impact the advanced devices.[2, 3] One of the key issues is to integrate biological function into such smart material system which requires the control of displaying the nanoscale components and/or bioactive molecule in the correct or desirable orientation with predictable and tunable binding strength. So far in the literature, this has been done mostly by either non-specifically, i.e., random organization of the entity on the surface, or via synthetic linkers, such as thiols and silanes.

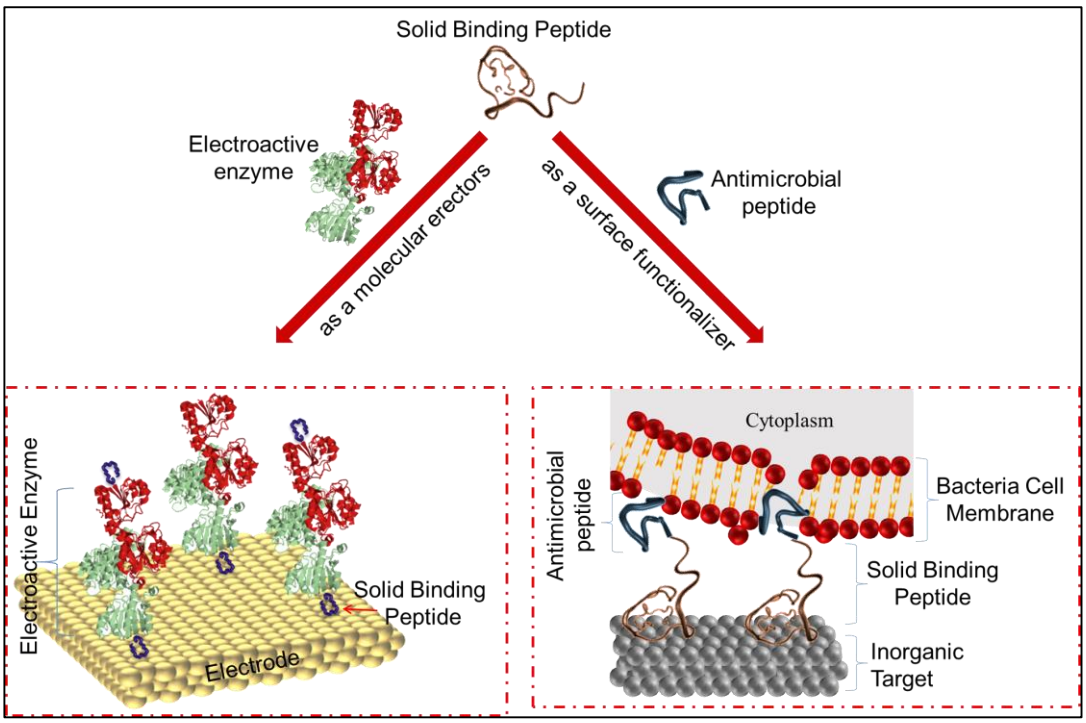

Figure 1: Utilization of GEPI as a molecular erector (left) and surface functionalizer (right) molecule.

Here, we propose to use specific solid binding peptides that can be further functionalized to create chimeric biomolecular constructs that not only binds to a given solid surface but also displays the desired biological functionality e.g., antimicrobial molecules, electrocatalytic enzymes (Figure 1). The first step toward this goal is the development of reliable molecular linkers and/or anchoring molecules for tethering the functional molecules on the inorganic support surface. During the last decade, combinatorially selected solid binding peptides have emerged as a novel alternative to the conventional surface functionalization and deposition techniques built upon their highly specific molecular recognition and binding properties as well as their ability to form densely packed monolayers on inorganic surfaces. In the scope of this thesis, we have investigated utilization of GEPI's as an anchoring molecule to functionalize surfaces while coupling the biological activity at the material interfaces by three different case studies.

1.1 Case Study I: Direct Bioelectrocatalysis at Interfaces using GEPI's

The functional integration of biomolecules onto solid material interfaces is attracting interests more than ever due to their impact on a diverse array of application areas.[1-5] Recent advances in translating the biomolecular mechanisms into the hybrid materials and system design promise novel methodologies that may transform some of our engineering approaches.[6-13] One of the major challenges in such systems is to have control at the bio-nano-material interface. Biomolecules need to be integrated at the material interfaces without compromising their spatial distribution, organization and orientation-dependent activity within a desired proximity.[3,4,7,12] Among Nature`s indispensable repertoire, enzymes owing to their exquisite catalytic features are certainly one of the most appealing candidates to be utilized as an internal component in next generation devices.[9,12,14] However their spatial distribution with the desired orientation on the solid surfaces as well as operational stability and long-term reuse are among the critical parameters limiting their wide range integration to functional materials.[2,10-15] There is an urge to develop biological surface functionalization approaches that will allow the control desired functions at the bio-nano material interfaces with tunability over the multitude of scales.

Physical adsorption is one of the simplest ways to immobilize enzyme molecules onto support surfaces. However, controlling the interactions between the adsorbed molecule and the surface is difficult due to the weak and the nonspecific nature of the attachment process.[16-18] Chemical coupling providing a more stable interfacial interaction is a widely used immobilization strategy.[19-21] Self-assembled monolayers (SAMs) have been the indispensable approach to functionalize the

metallic surfaces for attaching any type of biomolecules. Here, the covalent linkage between a surface and molecule is formed by monolayers of alkane chains containing different functional groups, dependent upon the surface chemistry of the support material and the biomolecule.[22-24] Specifically, utilization of the monolayers of alkane-thiolates, containing carboxylic acid or amine terminal groups, is well documented for gold surfaces.[22] Despite the enhanced stability of the coupling interaction, a major drawback of this approach is the low retention of enzyme activity due to the randomly introduced covalent linkages during the coupling reaction. Once formed, those covalent linkers establish very rigid attachments and prevent the immobilized biomolecules from positioning themselves toward their substrates and/or cofactors.[19,22,25] Due to the structurally anisotropic nature of the enzyme molecules, lack of orientation control prevents the utilization of the enzyme's full potential, especially for bioelectric and biofuel cell devices.[26] Furthermore, single-layered supports such as graphene, are highly sensitive to the SAM-based surface activation methods, which may dramatically disrupt its unique electronic properties.[27,28] The realization of next generation hybrid devices integrated with biomolecules requires to develop more efficient immobilization methods. These techniques should provide better communication between the biological molecules and their solid surfaces built upon controllable interactions starting at the interfaces.

Over the last decade, combinatorial biology based selection methods for solid binding peptides have gained attention as a novel alternative to the conventional surface functionalization and deposition techniques, owing to their ability to bring specific biomolecular recognition and binding properties onto inorganic surfaces.[1-4,29-31] Moreover, the ease of genetic incorporation of these short sequences into any permissive site or the C- or N-terminus of an enzyme makes them an attractive option to the design of novel biomolecular systems featuring desired multifunctional properties.[3,5,15,32] This opportunity presents many novel aspects to alter while designing next-generation molecular systems through biological self-assembly. So far, we, and other groups, have designed and verified the abilities of various peptides as well as proposed many techniques to better understand the related molecular mechanisms leading to controlled interactions at the interfaces.[29-36] Also, several research groups, including ours, have demonstrated the use of a variety of solid binding peptides as anchoring molecules onto the surfaces as well as providing functional integration between the enzymes/proteins and specific inorganic supports.[32-40] The biological nature of these short peptide sequences and their vast ability to create self-organized

assemblies on a surface under physiological conditions make them highly desirable, when compared to their counterparts that may require higher temperatures and pH values, or other harsh reaction conditions.

Oxidoreductases are among the industrially important enzymes capable of catalyzing key metabolic reactions. These metabolic processes are classified as redox reactions that involve oxidation or reduction of substrate molecules as well as with a concomitant transfer of electron pairs between organic substrates and the specific cofactor molecules.[41,42] Dehydrogenases produce pure chiral molecules with their enantioselective oxidative and reductive catalytic properties. This property promotes these enzymes as highly valuable tools in the pharmaceutical, chemical, agriculture, and food processing industries. Nicotinamide adenine dinucleotide (NAD^+)-dependent formate dehydrogenase (FDH, EC 1.2.1.2) is an important member in the oxidoreductase family. After the break down of formate by NAD^+-dependent dehydrogenases at a close proximity of gold electrode, electrochemical reduction of NAD^+ to NADH takes place. The difference in redox potentials between gold electrode and NADH will lead to further electrochemical oxidation and as a result two electrons are transferred to the circuit. Due to its ability to regenerate NADH cofactor via an irreversible reaction using a considerably cheaper substrate, FDH is employed in NAD+/NADH regeneration processes.[43] Furthermore, FDHs have been used for sensing applications to detect formate quantitatively as an important fermentation product of aerobic and anaerobic bacteria.[44,45] The capability to transfer electron pairs between specific substrates and NAD^+ molecules offers another interesting potential for FDHs as such to power bioelectronic devices.[46] The industrial importance of NAD^+-dependent FDH has led researchers to develop different kinds of immobilization strategies through a variety of support materials to efficiently enable the desired use of the enzyme.[47-49] FDHs have been successfully isolated and produced from many different species, but methanol-consuming yeast species, such as *Candida methylica,* have received the most attention due to the enhanced stability and relatively high activity of their isolated NAD^+-dependent FDHs.[45,50,51]

In this study, we genetically engineered NAD^+-dependent formate dehydrogenase from *Candida methylica* to couple with gold binding peptide as a novel enzyme with chimeric properties. The resulting fusion enzyme was demonstrated to retain the catalytic activity both in solution and surface immobilized form while gaining additional self-organization ability verified on a variety of gold electrode surfaces.

1.2 Case Study IIA: Chimeric Peptides with Antimicrobial Properties as Implant Functionalization Agents for Titanium Alloy Implants

Titanium and its alloys have been extensively used in orthopedic and dental implants, mainly due to their unique combination of excellent mechanical properties, corrosion resistance, biocompatibility and osseointegration.[47-51] However, the risk of failure of these implants, which often entails severe clinical outcomes, still poses a significant threat to patients and clinicians.[52, 53] Although the recent enhancements in the design of prosthetic devices and the advancements in surgical procedures have reduced the number of complications leading to failure, implant associated bacterial infections is still a serious challenge and the major cause of post-surgical morbidity and mortality.[54]

Implant materials provides an ideal surface to the growth of common pathogens such as *Staphylococcus aureus*, *Staphylococcus epidermidis,* and *Pseudomonas aeruginosa*, which could acquire shortly after surgery or at later stages of implantation. Failure to adequately combat these bacterial infections at implant-tissue interface often results in complex revision procedures as well as economic burden in health-care system, and in most cases the removal of the implant is the only remedy. Moreover, formation of complex biofilm structures by these pathogens on the surface of implant and its periphery often makes the problem more difficult to address. By forming a barrier against other molecules in the local microenvironment, these bacterial biofilm structures significantly decreases the susceptibility of infectious organisms to antimicrobial agents due to poor penetration rates.[52, 55, 56]

Even though the efforts of local delivery of systemic antibiotics through implant surfaces has received substantial interest as a promising treatment strategy, challenges regarding diluted levels of drug concentration at the target site and the potential toxicity of conventional antibiotics are still need to be addressed.[56, 57] Furthermore, the potential development and spread of antibiotic-resistant pathogens such as the methicillin-resistant *Staphylococcus aureus* (MRSA) is another concern which may lead to devastating effects on society.[56, 59]

An optimal design of a non-adhesive and infection resistant surface coatings using alternative antimicrobial agents with a broad spectrum antibacterial activity would be a preferred solution for this problem. Several surface coating and functionalization strategies have been reported to overcome implant failure associated with infections. In an attempt to render the non-adhesive and/or antimicrobial resistant surfaces, the use of polyethylene glycol (PEG) and its derivatives[60,

[61], coatings of albumin[62], covalent attachment of conventional antibiotics[63-66], chlorhexidine[67], silver, nitrogen oxide[68, 69] and quaternary ammonia compounds[65, 70] have been demonstrated. While the activation of implant surfaces by these agents have been shown to reduce bacterial adhesion, existing covalent coupling strategies often require the presence of specific functional groups on the surface with complex optimization steps. Moreover, the limited capacity of these functional groups to be used for modification of a different materials make them far from being a comprehensive solution.[71-73] Additionally, the slow release of these antimicrobial agents through the preloaded implants at the site of infection has raised concern about a possible link to increased bacterial resistance and cytotoxicity.[74]

Bioactivation of implant surfaces with more biocompatible and nontoxic biomolecules having an antibacterial property would be a feasible approach to successfully overcome infection derived implant failure without evoking toxicity and leading to antibiotic resistance. In this regard, utilization of antimicrobial peptides (AMPs) would be a preferred solution. These short, cationic antimicrobial agents are evolutionary conserved constituents of the immune defense of many organisms including insects, plants, and animals.[75-77] These are also believed to specifically target and disrupt the integrity of negatively charged cell membrane of microorganisms. Although there is no consensus in their sequence and structure, AMPs can easily adopt to an amphipathic structure and thereby the efficient molecular recognition between the cationic residues of peptide and the phospholipids of the bacteria membrane is promoted.[78, 79] Furthermore, in contrast to conventional antibiotics, it is extremely difficult for microorganisms to develop resistance against these peptides because of their highly sophisticated reaction mechanisms and considerably rapid rate action.[75, 80] More importantly, AMPs have broad-spectrum antimicrobial activity against gram-positive and gram-negative bacteria, fungi and viruses. Working synergistically with conventional antibiotics, they facilitate the penetration of antibiotics to the infection site, and provides more aggressive treatment against biofilms.[75] It has been also demonstrated that the sequence and resulting structure of natural AMP's can be utilized as templates for designing synthetic variants with enhanced antimicrobial activities.[81-83] The use of AMP's as an antimicrobial surface coating agents by tethering and assembling as a thin layer would also help to prevent their distribution along the bloodstream and potential cytotoxic consequences.[84]

In course of this study; unlike other approaches utilizing covalent linkages to tether AMPs on implant surface, we have created chimeric peptides composed of solid binding peptide[23] motif and

an AMP motif. These chimeric peptides rely on the titanium-binding properties that preferentially bind to the titanium surface as the most common implant surface and a freely exposing AMP to combat invading bacteria. With this aim, chimeric peptides were constructed by combining combinatorially selected solid binding peptides with AMP sequences in different combinations with a flexible linker in between.[85-88] These chimeric peptides were characterized in terms of their binding properties to titanium surface and their antimicrobial efficacy both in-solution and on surface. Keeping in mind the importance of assessing any therapeutic target against a range of problematic bacteria due to varying responses, we chose two different types of bacteria (*Staphylococcus epidermidis and Escherichia coli*) to test the efficacy of chimeric peptides against them. *S. epidermidis* is a gram-positive, biofilm-forming bacterium commonly found in orthopedic implant infections, making up 32% of clinical isolates from orthopedic implant infections and *E. coli* is a gram-negative, slime-producing bacterium sometimes found in orthopedic implant infections.[89-91]

The aim of this research is to develop an alternative method of implant-surface functionalization that does not require complex procedures or the covalent modification of the implant surface.[91-93] The principles laid out here can be applied to other identified AMP sequences, and expanded to biomaterials rather than titanium surface by using different solid binding sequences that binds to other biomaterials.[23, 93, 94]

1.3 Case Study IIB: Tunable Bioactive Interface Design for Zirconia Based Implants

The application of dental implants has been considered as a well-accepted treatment modality in restoration of function after the tooth loss in modern dentistry and provides considerably more comfort than dentures or bridges for patients. [95, 96]

Among different materials, titanium and its alloys have been the most commonly used material in oral prosthetics until now. Biomedical zirconia-based ceramics have however been proposed as a viable alternative to titanium with their exquisite mechanical and chemical properties as well as its high biocompatibility. [95, 97-99] The dimensional stability, high fracture toughness and extensive mechanical strength make zirconia-based ceramics the material of choice for dental prosthetic applications.[100, 101] Furthermore, the growing interest for zirconia in prosthodontics can also be attributed to their optical properties which can better mimic the ivory-like color of natural tooth than the gray titanium.[102, 103] Moreover, the non-allergenic nature of zirconia is another advantage of using zirconia to replace metals and metal alloys in restorative dentistry. [97, 104]

However, despite reports of high success rates in dental implants (more than 89%) the risk of failure of these implants, which often entails severe clinical outcomes, still poses a significant threat to patients and clinicians.[52, 53, 102, 105]

One of the most common problem associated with early failure of dental implants is bacterial infection that usually initiates by the adhesion of initial colonizers on implant surface and the surrounding soft tissue.[106] Colonization of dental implant by natural mouth flora starts immediately after the exposure of implant to the oral environment and eventually evolves into a complex biofilm structure consisting of variety of periodontal pathogens.[105, 107-110] These structures are highly resistant to many antimicrobial agents, e.g. antibiotics, disinfectant chemicals, as well as natural components of the defense system of the body.[111] Therefore, the initial adhesion and early-colonization of bacteria on implant surface is a critical step to prevent bacterial invasion and infection related implant failure.[112]

Coating the implant surfaces with a non-adhesive and infection resistant materials is considered as a very promising strategy for this problem. Such coatings allow high local antimicrobial agent concentrations which is impossible to reach with conventional antibiotic treatments where the dilution effects of biofilms are keeping systemic antibiotic levels below the minimum effective concentration values.[113] Approaches for rendering infection resistant implant surfaces includes antibiotic releasing coatings[114], the use of polyethylene glycol (PEG) and its derivatives[60, 61], covalent attachment of conventional antibiotics[63, 65], chlorhexidine[67], Ag/Zn modification[115, 116]. Among these, the utilization of infection resistant surface coatings displaying antimicrobial peptides (AMPs) with a broader spectrum of antibacterial activity compared to conventional antibiotics has attracted much attention.

One of the major advantage of antimicrobial peptide over conventional antibiotics is their rapid rate of action against microorganisms. These molecules utilize highly sophisticated reaction mechanisms and therefore developing the resistance against these peptides is very difficult. Furthermore, AMPs exert a broad spectrum of antimicrobial function against gram-positive and gram-negative bacteria, fungi and viruses. In addition to their superior antimicrobial characteristic, these molecules can also work with conventional antibiotics synergistically to provide more aggressive treatment against biofilms.[75-80]

In this study; unlike other approaches requiring utilization of additional synthetic covalent linker and extensive chemical surface activation to tether AMPs on implant surface, we have created

chimeric peptides having zirconia surface recognition and binding ability as well as antimicrobial functionality. These chimeric peptides self-recognizes the implant and forms a continuous coating layer on the surface while freely exposing the antimicrobial motif to combat invading bacteria. Next, binding properties and antimicrobial functionality of these chimeric peptides were characterized in-solution and on implant surface. Gram-positive, biofilm-forming *Streptococcus mutans*, which is the most common cariogenic organism found in oral flora was used to test the efficacy of developed peptide based implant coating.[117]

2. Materials and Methods

2.1 Case Study I: Direct Bioelectrocatalysis at Interfaces using GEPI's

2.1.1 Materials

The pDrive and pQE2 (Qiagen, USA) vectors were used as a cloning and expression vectors, respectively, and *Escherichia coli* strain DH5α-T1 (Invitrogen, USA) was selected as a host organism for both studies. Ampicillin and bacterial media supplements were obtained from Sigma–Aldrich. Ni-NTA (Qiagen, USA) and Glutathione Sepharose (GE Healthcare, USA) affinity matrices were used for protein purification. Chemicals used in buffer preparations were purchased from Sigma–Aldrich. NAD^+ (Roche, USA) and sodium formate were used for enzyme activities measurements. Binding studies were done using gold-coated SPR slides (Reichert Technologies, USA).

2.1.2 Cloning of cmFDH and the cmFDH-AuBP2 fusion enzymes

The *cm*FDH gene was obtained in the pQE2 vector and used as a template for cloning both the *cm*FDH and the *cm*FDH-AuBP2 fusion proteins.[46] The *cm*FDH and *cm*FDH-AuBP2 encoding DNA sequences were constructed using Polymerase Chain Reaction (PCR) by primers specifically designed to add *Pst*I and *Sac*I restriction sites to the N-terminus and C-terminus of the protein coding region, respectively. AuBP2 (CGPWALRRSIRRQSYGPC) peptide coding region was inserted to the N-terminus of the protein by using double step PCR using two different primer sequences (see supplementary information for primer sequences). The resulting PCR amplified protein coding sequences were first sub-cloned into the pDrive cloning vector and then transferred into the pQE2 expression vector. They were ligated using a rapid Roche DNA ligation kit (Figure 2(a) and 2(b)). Finally, PreScission Protease recognition site was inserted between the poly (His) tag (Figure 2(c) and 2(d)) and the protein coding region using specifically designed primers (see Appendix A for primer sequences) in combination with the Gene-Tailor site-directed mutagenesis kit (Invitrogen, USA). This modification allowed us to achieve the removal of poly (His) tag via PreScission Protease. Resulting constructs were transformed into the expression host *E. coli* DH5α-T1 cells via chemical transformation.

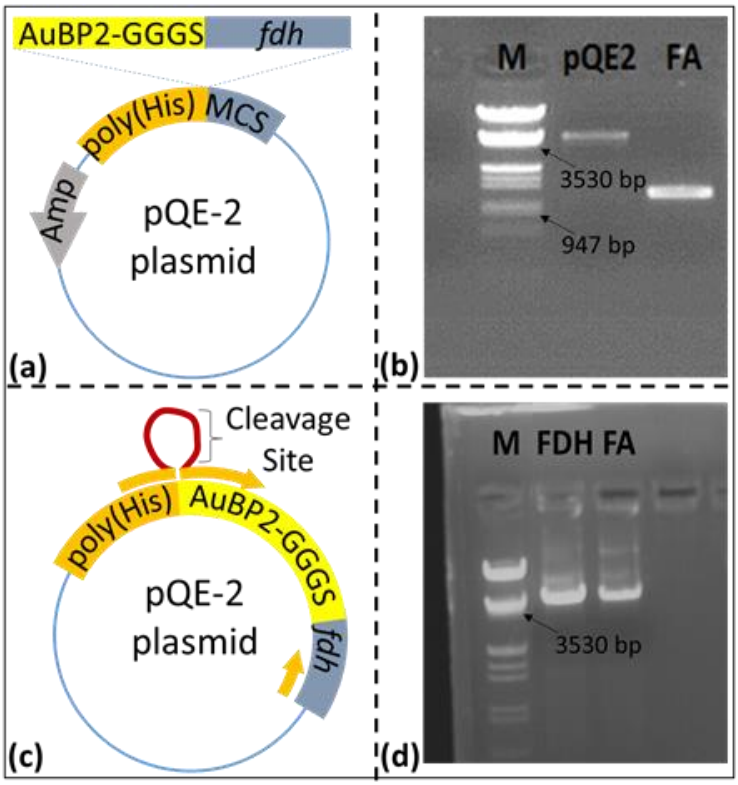

Figure 2: (a) Schematic diagram of vector construction of the cmFDH-AuBP2 fusion protein. (b) Agarose gel images of Lambda DNA marker (M), PstI and SacI digested pQE2 vector (pQE2) and cmFDH-AuBP2 (FA). (c) Schematic diagram of vector construction of the cmFDH-AuBP2 fusion protein with protease recognition site. (d) Agarose gel images of Lambda DNA marker (M) and, PCR products of the pQE2-cmFDH (FDH) and pQE2-cmFDH-AuBP2 (FA) vectors after site-directed mutagenesis reactions.

2.1.3. Expression of cmFDH and the cmFDH-AuBP2 enzymes

The pQE2-*cm*FDH or pQE2-*cm*FDH-AuBP2 plasmids harboring cells were used for protein expression studies. Cells were first grown overnight at 37°C in 5 ml of Luria Bertani (LB) media, containing 100 µg/mL ampicillin. Next, 1 ml of overnight culture was inoculated into fresh LB media and incubated at 37°C until it reached an optical density (OD_{600}) 0.5. Protein expression was induced with isopropyl β-D-1-thiogalactopyranoside (IPTG) addition to a final concentration of 0.5 mM and the culture was incubated for 16 hours at 16°C with constant agitation (200 rpm). Cells were then harvested following the QIA expression manual (Qiagen, USA) and re-suspended in sodium phosphate buffer (50 mM NaH_2PO_4, 300 mM NaCl, 20 mM imidazole, pH 8.0)

containing 0.5 mM phenylmethanesulfonyl fluoride (PMSF). Cells were lysed by 1mg/mL lysozyme treatment for 30 minutes on ice and sonicated at 200 W 3 times for 10 seconds. Finally, resulting cell lysate was centrifuged and the supernatant solution was reserved for further purification.

2.1.4 Purification of cmFDH and cmFDH-AuBP2 enzymes

The similar affinity purification method, i.e. nitrilotriacetic acid (Ni-NTA) metal-affinity chromatography, was used to purify the *cm*FDH and *cm*FDH-AuBP2 enzymes. Pre-packed Ni-NTA column was first equilibrated with sodium phosphate buffer (50 mM NaH_2PO_4, 300 mM NaCl, 20 mM imidazole at pH 8.0) and then the total protein containing supernatant solution was loaded into the column. Non-specifically bound proteins were removed by applying five column volumes of sodium phosphate buffer (50 mM NaH_2PO_4, 300 mM NaCl, 50 mM imidazole at pH 8.0) containing 1% Triton X-100 solution. Proteins of interest were eluted by increasing the imidazole concentration in the sodium phosphate buffer up to 250 mM. Finally, the purification process was confirmed by the sodium dodecyl sulfate polyacrylamide gel electrophoresis (SDS-PAGE) analysis.

2.1.5 Affinity tag (His-tag) removal from enzymes

The enzymes purified in sodium phosphate buffer were first exchanged into 1X PreScission Protease cleavage buffer (50 mM Tris-HCl, 150 mM NaCl, 1 mM EDT, 1 mM DTT, pH 7.0) using 30000 MWCO ultra-filtration centrifugal device (Amicon, USA). The histidine-tag cleavage reaction was then performed using a previously described protocol[33]. Both tag-free *cm*FDH or *cm*FDH-AuBP2 enzymes were obtained in 20 mM Tris-HCl buffer at pH 8.0 followed by purification of respective protein solutions via Ni-NTA and glutathione-Sepharose resins using similar conditions described above.

2.1.6 Enzyme activity measurements

The steady-state enzyme activity measurements were carried out at 25°C in a reaction mixture containing 20 mM Tris-HCl buffer at pH 8.0, 1 mM NAD^+, 0–40 mM formate, and 0.4 μM enzyme in a total reaction volume of 1 ml. The increase in absorption at 340 nm, corresponding to the reduction of NAD^+, was monitored and data was analyzed using an enzyme kinetics tool, GRAFIT software (Version 5.0.13, Erithacus Software Ltd, Horley, Surrey, UK). Data was reproduced three

times and all assays were performed in triplicates. The enzyme concentration was determined by Bradford assay using bovine serum albumin (BSA) standards, at 595 nm wavelength.

2.1.7 Surface binding kinetics measurements

Binding kinetics of *cm*FDH and *cm*FDH-AuBP2 enzymes were performed using a single channel SPR instrument (Kretschmann configuration) developed by the Reichert Instruments. Buffer solutions were degassed to avoid bubble formation in the flow cell. After establishing a stable baseline signal by flowing 20 mM Tris-HCl buffer, pH 8.0 over the surface, *cm*FDH or *cm*FDH-AuBP2 enzyme solutions in given concentrations were flowed through the surface, and their adsorption was monitored. The temperature within the flow cell of the SPR was kept at a constant 25°C via a heating element and a cooling fan controlled by a temperature sensor. All of the solutions used were introduced to the flow cell at a rate of 100 µl/min. In our data analysis, the Langmuir isotherm model was used to calculate the association (k_a), dissociation, and equilibrium constants (K_{eq}) of the adsorption process at different enzyme concentrations.

2.1.8 Enzyme activated electrode experiments

To create an enzyme-activated electrode system, we first obtained 525 µm thick silicon wafers coated with 100 nm Au layer. As an adhesion layer between gold coating and silicon wafer, titanium having 5nm thickness was used (Platypus Technologies, Madison, WI).The gold coated substrates were cut in 1cm x 1cm dimensions to be utilized as gold electrodes. Molecules of *cm*FDH-AuBP2 enzyme were next adsorbed onto one of the electrodes to activate the gold surface. For adsorption process a 200 µl of 10 µM *cm*FDH-AuBP2 enzyme in 20 mM Tris-HCl buffer, pH 8.0, was applied onto a gold surface and incubated for 15 minutes in a humidity chamber at room temperature. The enzyme-immobilized electrode was subsequently washed with Milli-Q water to get rid of excess proteins from surface before placed into a sterile beaker in parallel with the bare gold electrode. This design acted as an electrochemical cell after the beaker was filled with 20 mM Tris-HCl, pH 8.0 and 0.1M KCl until both electrodes were submerged. A 22 KΩ resistor was attached to the lead of the electrodes. Output voltage of cell was measured by an HP 974A Multimeter.

2.2 Case Study IIA: Chimeric Peptides with Antimicrobial Properties as implant Functionalization Agents for Titanium Implants

2.2.1 Target material Characterization and Preparation:

Surface properties of titanium grade V powder (Sigma-Aldrich, USA) and titanium grade V implant (Vetimplants, USA) were determined by scanning electron microscopy (SEM). Moreover, elemental composition of substrates were analyzed by collecting EDS spectra for 100 seconds at 9 keV using a LaB_6 filament. Titanium grade V implant was cut into approximately 1cm x 1cm squares and sharp edges were removed by hand polishing with a 600-grit finish silicon carbide metallurgical paper. Before proceeding any experiment, titanium grade V powder and implant pieces were cleaned by sonicating sequentially in a 1:1 acetone/methanol mixture, then isopropyl alcohol, and finally de-ionized water. Then, substrates were sterilized for 15 minutes via UV irradiation.

2.2.2 Selection of Titanium Binding and Antimicrobial Binding Peptides:

Titanium binding peptides (TiBP) that are previously selected by cell surface display method[94] were pooled together with the peptides that were selected in this study using phage display approach. Briefly, for cell surface display approach, the FliTrx bacterial cell surface display system (Invitrogen, USA) was used to select peptide sequences against titanium substrates.[118-120] After four rounds of successful biopanning process, the enriched DNA nucleotide sequences of each of the 60 isolated clones were analyzed. Then, binding properties of each peptides were characterized by quantitative fluorescence microscopy employing a Nikon Eclipse TE-2000U fluorescence microscope (Melville, NY) equipped with a Hamamatsu ORCA-ER cooled CCD camera (Bridgewater, NJ), imaged using a FITC filter (exciter 460–500 nm, dichroic 505 nm, emitter 510–560 nm) and METAMORPH software (Universal Imaging, USA). Finally, binding affinity of each clone was determined by calculating the average number of adherent cells on the titanium surface in triplicate samples. Consequently, the TiBP were grouped as strong, moderate or weak binders, according to their binding level.

As described previously[121], in phage display, the Ph.D.-12 phage display peptide library kit (New England BioLabs, USA) containing 1.2×10^9 different randomized peptide sequences was used. First of all, the peptide library was incubated with titanium grade V powder in potassium PC buffer containing 0.1% Tween 20 detergent (Merck, USA) and then the unbound phages were removed by washing with PC buffer containing 0.1% detergent (Tween 20 and Tween 80, Merck).

Afterwards, the bound phages were eluted specifically from the surface using elution buffer; and the eluted phage pool is amplified in *Escherichia coli* ER2738. Amplified phages were then purified and subsequently used for additional panning rounds. After each round, the phages were grown on solid media, and single clones are selected by picking single-phage plaques. DNA of single-phage clones are then isolated and sequenced. Finally, individual clones were characterized by quantitative fluorescence microscopy employing a Nikon Eclipse TE-2000U as described above.

Computationally designed and characterized multiple AMP sequences are chosen by data mining from literature.[88, 122]

2.2.3 Peptide Synthesis:

An automated solid-phase peptide synthesizer (CS336X, CS-Bio Inc., Menlo Park, USA) was utilized to synthesize peptides through Fmoc-chemistry. In this approach, modified amino acids (Chempep, USA), where N-terminus and side chain of amino acids were protected by Fmoc group and an appropriate protecting group, respectively, were used. In the reaction vessel, the Wang resin (Novabiochem, USA) pre-loaded with F-moc protected first amino acid was treated with 20% piperidine in DMF to remove the Fmoc group, which was monitored by UV-absorbance at 301 nm. The incoming amino acid separately activated with HBTU (Sigma Aldrich, USA) in DMF was transferred into the vessel and incubated with the resin for 45 min. After washing the resin with DMF, the same protocol was applied for addition of the next amino acids.

Following the synthesis, the resulting resin-bound peptides were cleaved and side-chain-deprotected using Reagent K (TFA/thioanisole/H2O/phenol/ethanedithiol (87.5:5:5:2.5)) and precipitated by cold ether. Crude peptides were purified by RP-HPLC up to >98% purity (Gemini 10u C18 110A column). The purified peptides were confirmed by mass spectroscopy (MS) using a MALDI-TOF mass spectrometry with reflectron (RETOF-MS) on an Autoflex II (Bruker Daltonics, USA) mass spectrometer located in Department of Medicinal Chemistry at University of Washington. 4 mM stock solutions of each peptide were made in sterile de-ionized water by dissolving the peptides. Subsequent dilutions for experiments were done with sterile 1X PBS. Synthesized peptides were listed in Table 1. The molecular weight (MW), isoelectronic point (pI), charge and grand average of hydropathy (GRAVY) value parameters for each peptide were calculated using ExPASy Proteomics Server.

Table 1: MW, pI, net charge and the hydropathy of selected titanium binding peptides (TiBP).

Peptide Name	Sequence	MW (kDa)	pI	Charge	G.R.A.V.Y score
TiBPS1	RPRENRGRERGL	1495.6	11.82	+3	-2.633
TiBPS2	SRPNGYGGSESS	1197.1	5.72	0	-1.567
TiBPS3	HAYKQPVLSTPF	1387.6	8.60	+1	-0.333
TiBPS4	WSYESSTPRTQL	1454.5	6.00	0	-1.275

2.2.4 Binding Characterization of Peptides:

Similar fluorescence microscopy characterization procedure was applied to investigate binding affinities of both of the selected titanium binding and AMP conjugated chimeric peptides. Firstly, the biotinylated peptides were incubated with pre-cleaned substrates for 3 hours at room temperature. Following, substrates were washed with 1X PBS Buffer for three times and then bound peptides were labelled with Alexa Fluor 488 streptavidin probes by incubating for 15 minutes at dark. Following, substrates were washed with de-ionized water three times and bound peptides were visualized on the substrate surface using a Nikon Eclipse TE-2000U Fluorescence Microscope (with Hamamatsu ORCA-ER cooled CCD camera) using a FITC filter (exciter 460-500, dichroic 505, emitter 510-560) and METAMORPH Software (Universal Imaging, USA). Surface coverage ratios were determined by using METAMORPH Software. All measurements were carried out in triplicate experiments.

2.2.5 Bacterial Maintenance and Culturing:

Two bacteria species - *Escherichia coli* ATCC® 25922™ and *Staphylococcus epidermidis* ATCC® 29886™ were used in the present study. Both of them were cultured according to ATCC® protocol using the following media: Trypticase Soy Broth (TSB) (Fluka, 22092) for *E. coli* and Nutrient Broth (NB) (Difco 0003) for *S. epidermidis*. For all three bacterial species, the bacterial pellet obtained from ATCC was rehydrated in 0.5 mL of the above-specified media, and several drops of the suspension were immediately placed and streaked on an agar slant of the

specified media. The agar-plate was then incubated aerobically at 37°C for 24 hours. Overnight cultures of *S. epidermidis* and *E. coli* were prepared by aseptically transferring a single-colony forming unit into 10 mL of NB or TSB (respectively), followed by aerobic incubation at 37°C with constant agitation (200 rpm) for 16 hours.

2.2.6 In-Solution Antimicrobial Activity of Chimeric Peptides:

The in-solution antimicrobial activities of the peptides were analyzed against *S. epidermidis* and *E. coli* spectrophotometrically. For each bacteria species, solutions of selected antimicrobial peptides were added in specified media up to a specified concentrations and inoculated with the bacteria with a final concentration of 10^7 cells/mL. Bacterial growth at 37˚C was monitored over the course of 24 hours by optical density measurements at 600 nm on a Tecan Safire Spectrophotometer. For each experiment, a positive control consisting of solely 10^7cells/mL of bacteria in the specified media, and another negative control consisting of only media was monitored as well.

2.2.7 Bacterial Adhesion and Quantification on Peptide Coated Implant Surfaces:

Pre-cleaned titanium substrates were incubated at 37˚C under constant agitation (200 rpm) with peptide solutions for 3 hours. Following, the peptide solutions were removed from each well. 1 mL of sterile 1X PBS was then added to each well, pipetted up-and-down twice, and removed from the well. A second 1mL of sterile 1X PBS was then added to each well, pipette up-and-down once, and removed from the well. Using sterile forceps, each titanium substrate was moved to a clean well, free of any unbound peptides.

To proceed with bacterial adhesion experiments, overnight cultures for each bacterium were prepared as described above. Bacteria from the overnight cultures were used to inoculate fresh media to a final concentration of 10^7 cells/mL. Cultures were then incubated in the same manner as the overnight cultures until they reached the mid-log phase as determined by optical density measurement at 600 nm. At the mid log phase, the cultures were centrifuged at 4000 rpm for 5 minutes in a Sorvall® RC 5B Plus Centrifuge. The supernatant was removed and the bacterial pellet was re-suspended in 500 µL of specified media. This suspension was then transferred to a 2 mL centrifuge tube and centrifuged at 5500 rpm for 3 minutes in a Fischer Scientific accuSpin™ Micro Centrifuge. The supernatant was carefully removed and the bacterial pellet was re-suspended in sterile 1X PBS to a final concentration of 10^8 cells/mL. Then, 1mL of the 10^8

cells/mL cell suspension was added to each well containing a peptide-modified titanium substrate and incubated for 4 hours at 37˚C under constant agitation (200 rpm). After 4 hours incubation, first the bacterial suspension was removed then the surfaces were washed two times with 1mL of 1X PBS by pipetting. At the end of the experiment, adhered cells to titanium substrates were fixed with 500 µL of 2% glutaraldehyde for 30 minutes, followed by dehydration in a series of increasing alcohol baths. (50% ethanol for 10 minutes, 70% ethanol for 10 minutes, 90% ethanol for 10 minutes and followed by a 1 mL wash with 100% ethanol.) 500 µL of 5 µM SYTO9® Green Fluorescent Nucleic acid stain (Invitrogen, USA) was added to each well containing a substrate, protected from light, and incubated for 20 minutes. Substrates were then washed 3 times with 1mL of 1X PBS by pipetting the PBS up-and-down two times. Following, the substrates were secured onto a clean microscope slide and viewed under a Nikon Eclipse TE2000-U Fluorescence Microscope. Five random images of each surface were taken and analyzed for percent surface coverage using Meta Morph (Version 6.r6) software.

2.3 Case Study IIB: Tunable Bioactive Interface Design for Zirconia Based Implants

2.3.1 Target material Characterization and Preparation:

Surface characteristics and elemental composition of zirconium (IV) oxide powder (Sigma-Aldrich, USA) and zirconia implant grade disks (3M, Germany) were evaluated using scanning electron microscopy (SEM) and energy dispersive spectroscopy (EDS). As described previously, both substrate materials were cleaned by soaking and sonicating in the 1:1 acetone/methanol mixture, isopropyl alcohol, deionized water. Finally, all of the substrates were sterilized by UV irradiation for 15 minutes.

2.3.2 Selection of Zirconium Binding Peptides:

Zirconium binding peptides were selected by direct selection approach using pre-constructed biotinylated peptide library. To characterize zirconium recognition and binding properties, each peptide in the library were first incubated with sterile zirconium (IV) oxide powder for 3 hours at room temperature. After washing off the excess with 1X PBS Wash Buffer for three times, bound peptides were labelled with Qdot™ 605 ITK™ Streptavidin Conjugate probes (Life Technologies, USA). Finally, binding properties of each peptide were analyzed with respect to their substrate surface coverages using a Nikon Eclipse TE-2000U Fluorescence Microscope (with Hamamatsu ORCA-ER cooled CCD camera) equipped with a Qdot filter and METAMORPH Software

(Universal Imaging, USA). Surface coverage ratios were determined by using METAMORPH Software. All measurements were carried out in triplicate experiments. According to surface coverages, selected peptides were classified as strong, moderate or weak binders.

2.3.3 Bacterial Maintenance and Culturing:

Two different bacteria species were employed in the present study: *Escherichia coli* ATCC® 25922™ and *Streptococcus mutans* ATCC® 25175™. Stock and overnight cultures of each species were prepared according to suggested ATCC® protocols using Trypticase Soy Broth (TSB) (Fluka, 22092) and Brain Hearth Infusion (BHI) (Fluka, 22092) for *E.* coli and *S. mutans*, respectively. For aerobic growth (*E. coli* 25922), an overnight culture of E.coli was diluted 1:50 into a 250-ml conical flask containing 50 ml of TSB, and cultures were grown on a rotary shaker (200rpm) at 37°C until late exponential growth. For anaerobic growth (*S. mutans* 25175), cultures were similarly diluted and incubated, but the medium was incubated at 37°C in a 5% CO_2 atmosphere to a late exponential growth.

2.3.4 In-Solution Antimicrobial Activity of Chimeric Peptides:

The in-solution antimicrobial activities of the chimeric zirconia binding peptides were analyzed against *S. mutans* and *E. coli* spectrophotometrically. For this assay, each bacteria species were seeded into chimeric zirconia binding peptide containing media to a final concentration of 10^7 cells/mL. Growth of each species were monitored by measuring optical density of growth culture over the course of 24 hours using Tecan Safire Spectrophotometer.

2.3.5 Bacterial Adhesion Assay on Peptide Coated Implant Surfaces:

chimeric zirconia binding peptide coating of zirconia implant discs were accomplished by incubating each chimeric peptide with the pre-cleaned zirconia substrates at 37˚C under constant agitation (200 rpm) for 3 hours. Following, excess amount of unbound peptides were removed from the surface with sequential washing steps using sterile 1X PBS buffer. Zirconia implant discs with or without peptides coating layer were incubated with *S. mutans* culture consisting of 10^8 cells/mL for 4 hours at 37˚C. Then, adhered cells were fixed with 1% glutaraldehyde for 30 minutes and then dehydrated in an ethanol series (30%, 50%, 70%, 85%, 95%, and 100%; 10 min each).

Following, to determine the viability of adhered cells, 500 μL of 5 μM SYTO9® Green Fluorescent Nucleic acid stain (Invitrogen, USA) was added onto each substrate, protected from light, and

incubated for 20 minutes. After washing off the excess amount of staining solution, zirconia discs were secured onto a clean microscope slide and visualized. Five random images of each surface were taken and analyzed using Meta Morph (Version 6.r6) software.

3. Results and Discussion

3.1 Case Study I: Direct Bioelectrocatalysis at Interfaces using GEPI's

We genetically engineered a novel fusion enzyme, formate dehydrogenase (*cm*FDH), which demonstrates self-organization ability on a gold surface while retaining its inherent catalytic activity. Efficiency of the solid binding peptide enabled anchoring of *cm*FDH onto gold surfaces was investigated with respect to its solid binding ability as well as the overall enzyme activity by comparing the kinetic activity parameters of *cm*FDH-AuBP2 engineered enzyme to the control *cm*FDH. Furthermore, we demonstrated the oxidation of formate in the enzyme activated electrode system.

3.1.1 Genetically engineered cmFDH-AuBP2 fusion enzyme

A biocombinatorially selected and characterized gold binding peptide[124] (AuBP2) was used as a fusion partner to *cm*FDH. The AuBP2 peptide sequence was inserted between the poly (His) tag and the N-terminus of the *cm*FDH coding region using a GGGS (Glycine–Glycine–Glycine–Serine) spacer to allow for efficient peptide display (Figure 2). The resulting engineered protein thereby ensures that the gold binding peptide region is freely exposed to the environment without any restriction on its conformation as well as any potential interference with the enzyme.

To purify the expressed recombinant protein with high yields, we employed a poly (His) affinity tag based approach. It has been previously shown that the N-terminal histidine tag does not influence the activity of *cm*FDH.[40, 46] On the other hand, multi-histidine residues have a non-specific, yet considerable high affinity, to a variety of metal surfaces including gold. To avoid the unpredictable properties of poly (His) affinity tag on newly introduced specific gold surface recognition ability, both peptide-fused and control constructs were specifically designed by introducing a protease cleavage site at the end of poly (His) region. This extra design step in our cloning approach allowed for complete removal of the poly-histidine tag region from the protein. The PreScission protease recognition and cleavage sites were introduced to the final enzyme constructs using a site-directed mutagenesis strategy. The schematic representation of AuBP2 incorporated *cm*FDH, spatial organization of poly-histidine tag, cleavage site and gold binding peptide regions are depicted in Figure 3(a). The plasmids encoding *cm*FDH and *cm*FDH-AuBP2 proteins were successfully expressed in *E. coli* DH5α-T1 strains and purified using Ni-NTA matrices under native conditions. Purity and molecular weights of the expressed proteins were

analyzed by SDS–PAGE (Figure 3(b)). The protein bands indicating *cm*FDH and *cm*FDH-AuBP2 were observed approximately at 41 and 43.5 kDa, respectively referring to the expected molecular weights for both enzymes following the inclusion of new sequences.

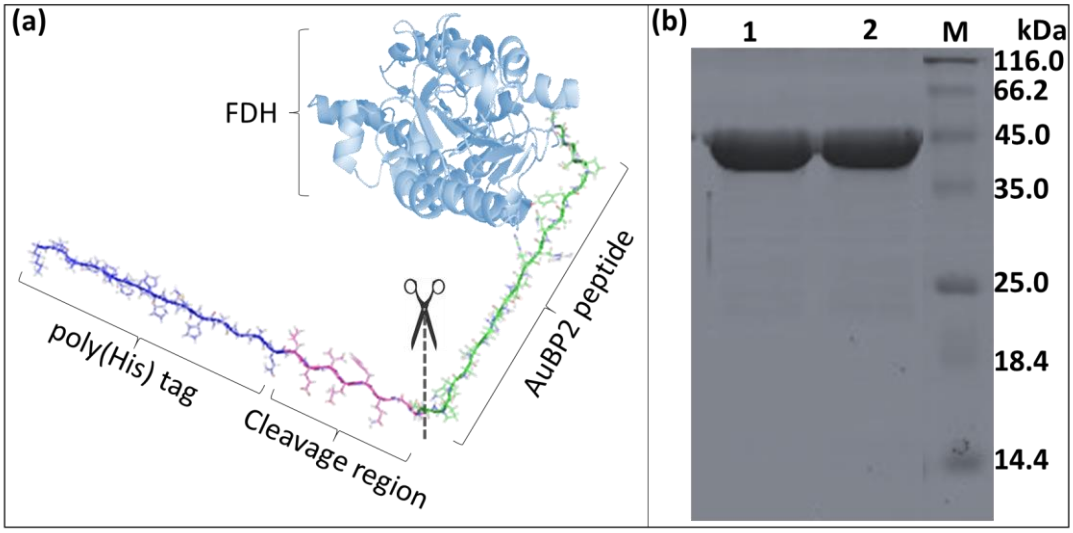

Figure 3: (a) Schematic display of constructed cmFDH-AuBP2 fusion protein with poly (His) tag and PreScission Protease cleavage sites (3D structure of FDH is adapted from PDB ID: 2J6I and recolored[125]). (b) SDS-PAGE image of purified enzymes after removal of poly (His) tag; lane 1: cmFDH and lane 2: cmFDH-AuBP2, M: protein weight marker with corresponding molecular masses.

3.1.2 Engineered enzyme activities

Upon the successful expression and purification processes, the catalytic activity of the wild-type and engineered enzymes were analyzed (Table 1). The unmodified wild-type *cm*FDH shows a similar catalytic activity ($0.592 \pm 0.019\ s^{-1}$) values when compared to other studies in the literature ($0.5 \pm 0.1\ s^{-1}$). This confirms that the inclusion of the new excision site to remove the poly-histidine tag from the enzyme did not affect the enzymatic activity.[46]

Many of the immobilization approaches explored so far result in a significant loss of catalytic enzymatic functionality, potentially due to the randomly introduced covalent bonds between the enzyme and the surface.[5, 8] In our case, we add a new functionality to the enzyme to attain surface functionalization ability, we first tested if the enzyme will retain its catalytic activity following the insertion of the new gold binding domain. The calculated enzyme kinetic parameters k_{cat}, which indicates the turnover rate of substrate to product, and K_m (the Michaelis constant), which describes an enzyme's affinity for its substrate, are provided in Table 2. The k_{cat} value obtained for the

cmFDH-AuBP2 (0.615 ± 0.021 s^{-1}) is very close to *cmFDH* (0.592 ± 0.019 s^{-1}) suggesting that the enzymatic breakdown of formate is similar for both enzymes. Furthermore, there is no significant difference attained in the substrate affinities (K_m) of *cmFDH-AuBP2* and *cmFDH*. The ratio of k_{cat}/K_m is an indicator of the overall catalytic efficiency of the enzyme. In our case, there is less than a 2% difference on the overall k_{cat}/K_m values between the wild-type and fusion enzymes. This difference is negligible enough to confirm that the apparent kinetic parameters of the wild-type *cmFDH* were not affected by the genetic fusion of AuBP2 and the enzyme activity was retained.

Table 2: Apparent kinetic parameters (Data represent mean ± SD).

	***cm*FDH**	**cmFDH-AuBP2**	**Pure FDH after digestion of His-tag[46]**
V_{max} (abs/min)	0.083 ± 0.003	0.092 ± 0.003	-
K_m (mM)	5.219 ± 0.689	5.549 ± 0.733	4.49 ± 0.6
k_{cat} (s^{-1})	0.592 ± 0.019	0.615 ± 0.021	0.5 ± 0.1
k_{cat}/K_m	0.113 ± 0.028	0.111 ± 0.028	0.1

3.1.3 Engineered gold recognition functionality of genetically engineered cmFDH-AuBP2

Here, we used SPR spectroscopy to characterize the binding of AuBP2 peptide tag, which was genetically inserted in the engineered fusion enzyme, *cm*FDH-AuBP2, on the gold surface and compared to the control, *cm*FDH. Figure 4 shows the schematic representation of single peptide adsorption onto a gold surface.

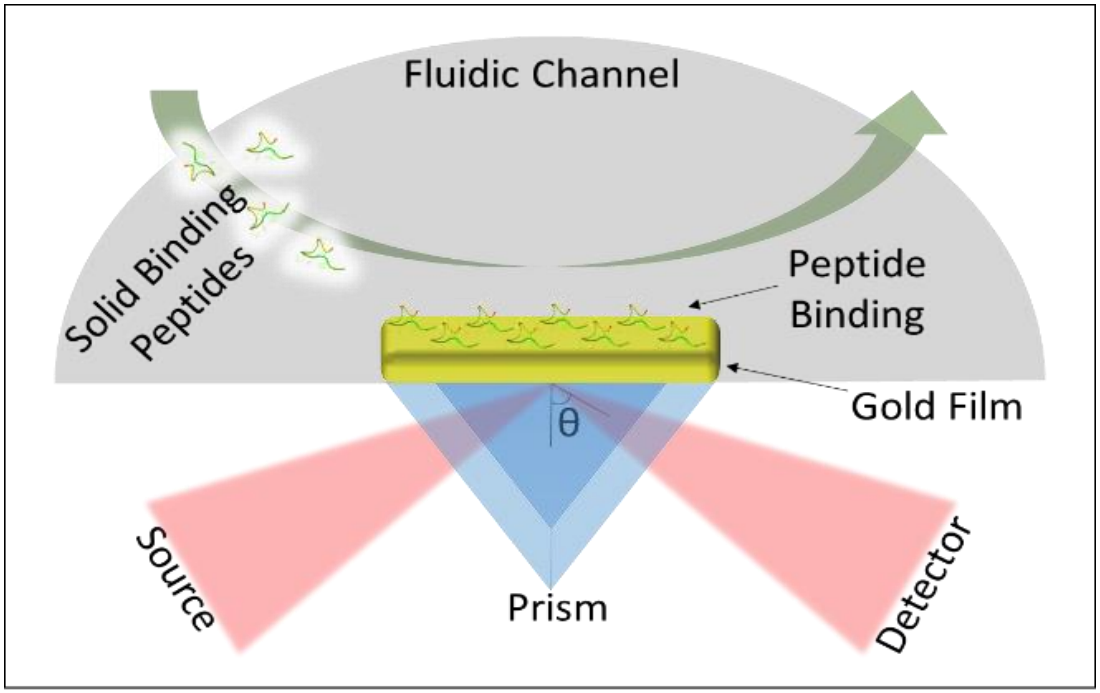

Figure 4: Schematic display of peptide adsorption on gold coated SPR chip.

Both enzymes were prepared at 0.25, 0.5, and 1 µM concentrations, and their respective SPR sensograms were recorded (see Appendix A for SPR sensograms). Then, the apparent binding rates (k_{obs}) of both enzymes were derived by nonlinear curve fitting to the Langmuir binding isotherm[123]. The kinetic adsorption and desorption parameters, given in Table 3, were calculated using a linear regression model (least-squares fit), according to the following equation:

[1] $$k_{obs} = k_a C + k_d$$

where k_a (slope) and k_d (intercept) are the association and dissociation rate constants, respectively, and C is the concentration. The equilibrium constant, k_{eq}, can then be calculated using the ratio k_a/k_d.[123]

The adsorption rate of the control protein (k_a of 2.38x10-3 $M^{-1}s^{-1}$), i.e. *cmFDH*, was considerably low for the gold surface, which can be attributed to non-specific interactions that are possibly caused by the presence of surface exposed histidine and cysteine residues. Even though these outer surface enzyme residues are known to interact with the gold surface, it is difficult to form a stable enzyme layer and thus the enzyme can be easily washed off of the surface. However, the effect of AuBP2 on the binding ability of fusion enzyme was drastic. Compared to the wild-type enzyme, there is approximately a 4.3-fold enhancement in the association rate constant and roughly a 3-

fold decrease in the dissociation rate constant, leading to a 13-fold increase in the equilibrium constant (K_{eq} of 15.564 M^{-1} compared to 1.214 M^{-1}).

Table 3: Binding constants of cmFDH and cmFDH-AuBP2.

	cmFDH	**cmFDH-AuBP2**
k_a x10^3 (M^{-1}.s-1)	2.38	10.35
k_d x10^3 (s^{-1})	1.96	0.665
k_a/k_d (M^{-1})	1.214	15.564
ΔG_{ads} (kcal/mole)	-0.115	-1.624

Figure 5(a) shows the surface affinities of the enzymes at 1 µM protein concentrations. At this concentration, maximum loading capacity of the sensor is estimated as 1.61ng/mm^2.Their adsorption differences indicate that the AuBP2 peptide tag provides an anchor for the fusion enzyme. Likewise, the standard Gibbs free energy (ΔG_{ads}) of adsorption (molarity representation) for both *cm*FDH and *cm*FDH-AuBP2 monolayers was calculated using the equation[123]:

[2] $$\Delta G_{ads} = -RTlnK_{eq}C$$

where K_{eq} is the equilibrium constant (k_a/k_d), C is the biomolecule concentration, R is the molar gas constant and T is the temperature in Kelvin. The ΔG_{ads} values for *cm*FDH and *cm*FDH-AuBP2 are found as -0.115 kcal/mol and -1.624 kcal/mol, respectively. These negative ΔG_{ads} values show the spontaneity of the interaction. The higher change in the standard free energy of adsorption for *cm*FDH-AuBP2 may be contributed to the fast binding process.

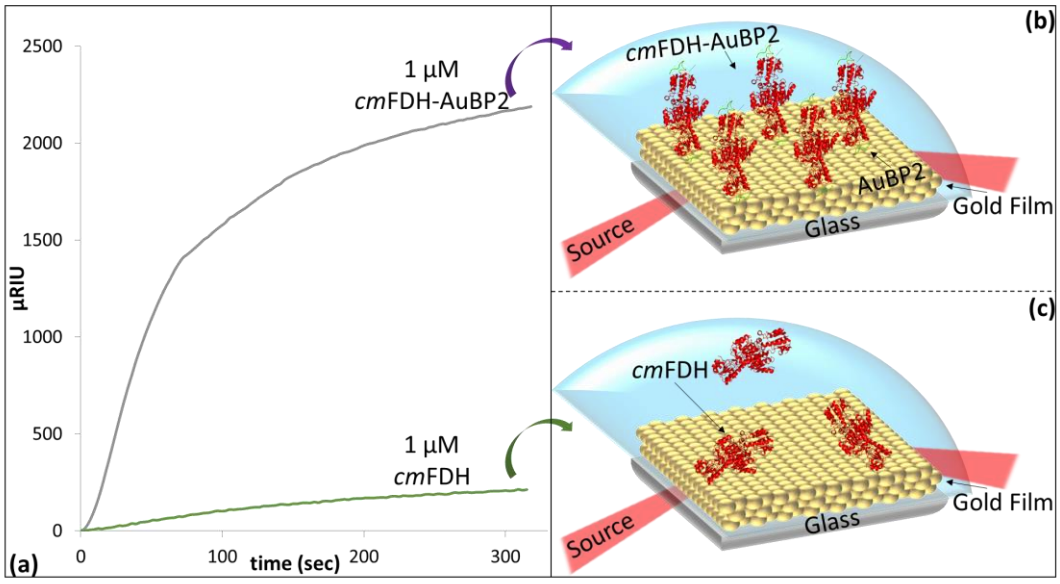

Figure 5: (a) Adsorption kinetics of constructed cmFDH and cmFDH-AuBP2 fusion proteins. Schematic display of binding characteristics of cmFDH-AuBP2 (b) and cmFDH (c) proteins on gold chip. (3D structure of FDH is adapted from PDB ID: 2J6I and recolored[125])

3.1.4 Engineered Enzyme Activated Sensor

The successful design of any enzyme-based device is dependent upon the efficiency of the immobilization strategy and the catalytic activity of the employed enzyme on its associated surface. With this aim in mind, the fusion enzyme, i.e. *cm*FDH-AuBP2, was immobilized onto a gold electrode surface and next tested for its catalytic activity. We monitored the conversion of formate to CO_2 electrochemically by designing a circuit-based system consisting of two gold electrodes submerged in solution (20 mM Tris-HCl buffer, pH 8.0, and 0.1 M KCl) and coupled the system with a 22 KΩ resistor used as a load. Figure 6 illustrates our experimental setup for monitoring the conversion of formate by the enzyme-activated gold electrode.

To activate the selected gold electrode, 10 µM of *cm*FDH-AuBP2 was applied on the surface. After allowing enough contact time with the surface, electrode was washed by buffer to get rid of excess enzyme which may not be contacting the surface directly but interfering with the protein film. The enzyme-activated electrode was then placed into a sterile beaker vertically, facing the bare gold electrode. The submerged gold electrodes were next connected in parallel to the resistor.

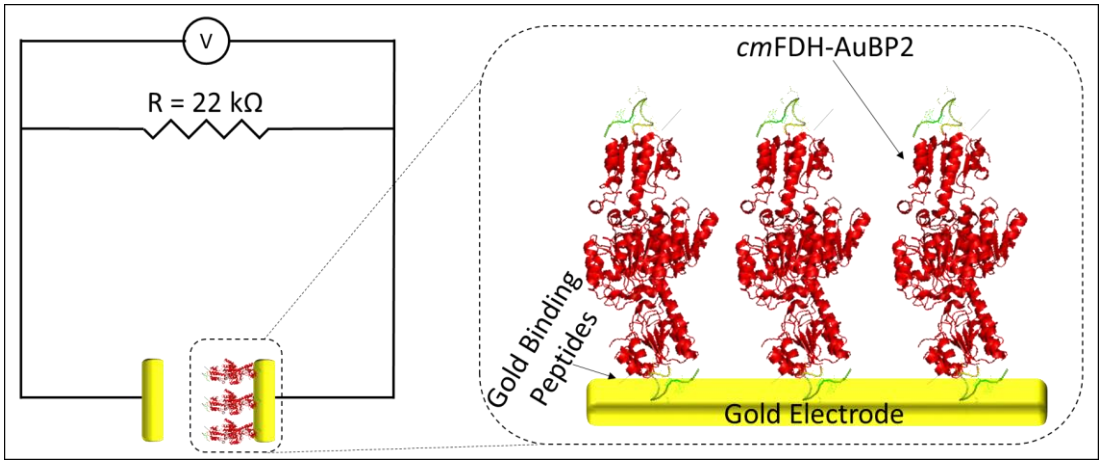

Figure 6: Schematic display of cmFDH-AuBP2 activated electrode design (3D structure of FDH is adapted from PDB ID: 2J6I and recolored[125]).

The observed potential difference (*V*, voltage) between the electrodes was read by a digital multimeter placed in parallel with the resistor. After establishing a baseline measurement, 0.25 mM formate as substrate and 1mM NAD^+ as the cofactor were added to the system and output voltage was monitored continuously. The energy released in the reaction due to the movement of electrons in the designed circuit gives rise to a potential difference equal to the electromotive force (emf, ε) .[126-127] The resulting change in current across the circuit elements was calculated by using Ohm's law equation (equation 3):

$$V = IR \quad [3]$$

where *V* is the potential difference measured across the resistor in units of Volts (V), *I* is the current through the resistance in units of amperes (A), and *R* is the resistance of the circuit in units of ohms (Ω).

The initial output voltage was first recorded as 270 mV, then resistor was connected to the system and consequent voltage drop was observed. Next, 0.25 mM formate and 1mM NAD^+ were added to the solution (~230mV) to monitor the enzyme based electrochemical conversion (Figure 7). Herein, the enzyme catalyzes the formate oxidation by NAD^+ until all formate is converted into its products of CO_2, NADH, and H^+ are produced. The electrons conducted through wire resulted in a rise in the voltage to about 250 mV. Consecutive additions of formate resulted in approximately 10% increase in the output voltage, which was maintained over a 10 minute period. Then, a decrease in the output voltage was observed following the complete conversion of the formate. The system showed relatively with range of pH and temperature stability, 6-9.5 and 16-

40^{o}C, respectively. The activity was shown to be preserved after five cycles. Overall our results demonstrate the catalytic capability of the immobilized enzyme using a bio-engineered circuit design. Our results also indicate the potential of extending the duration of output voltage as well as current by subsequent formate addition over multiple cycles. The circuit design can be further improved by optimizing the physical layout and electrical connections as well as individual components e.g. enzyme load, formate, internal and external resistances introduced to the system. Potentially, bio-enabled circuit based sensor system can be used for formate detection or NADH regeneration from NAD^+ by pharmaceutical and agrochemical industries.

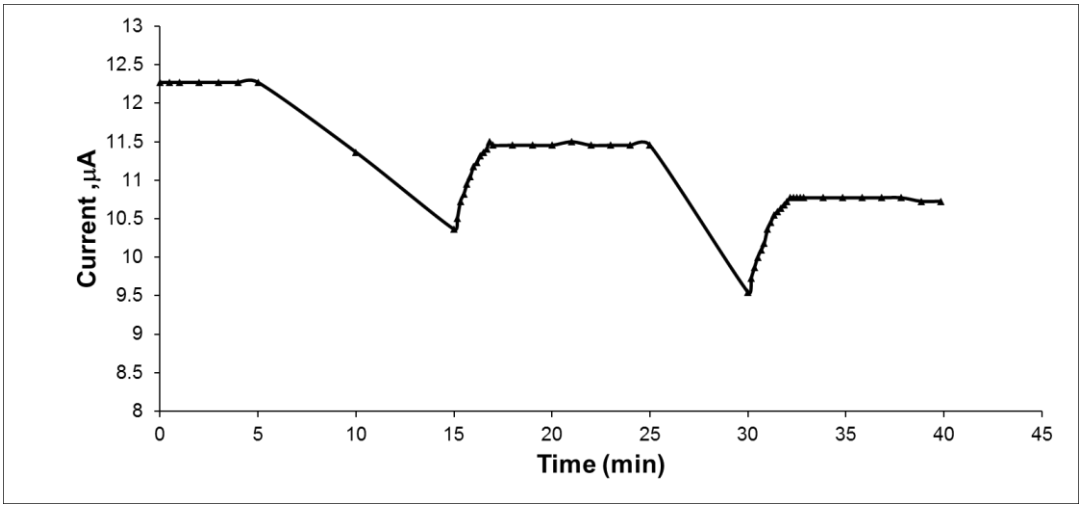

Figure 7: Change in total current output in response to time.

3.2 Case Study IIA: Chimeric Peptides with Antimicrobial Properties as Implant Functionalization Agents for Titanium Alloy Implants

In this study, we demonstrated the use of chimeric peptides as an antimicrobial coating agent on titanium grade V implants (Figure 8). Chimeric peptides, compromising combinatorially selected titanium binding region and computationally designed antimicrobial region, were constructed. Surface binding characterization of these peptides were investigated using FM. Furthermore, antimicrobial activity of these chimeric peptides were demonstrated against different pathogens; *S. epidermidis*, and *E. coli*.

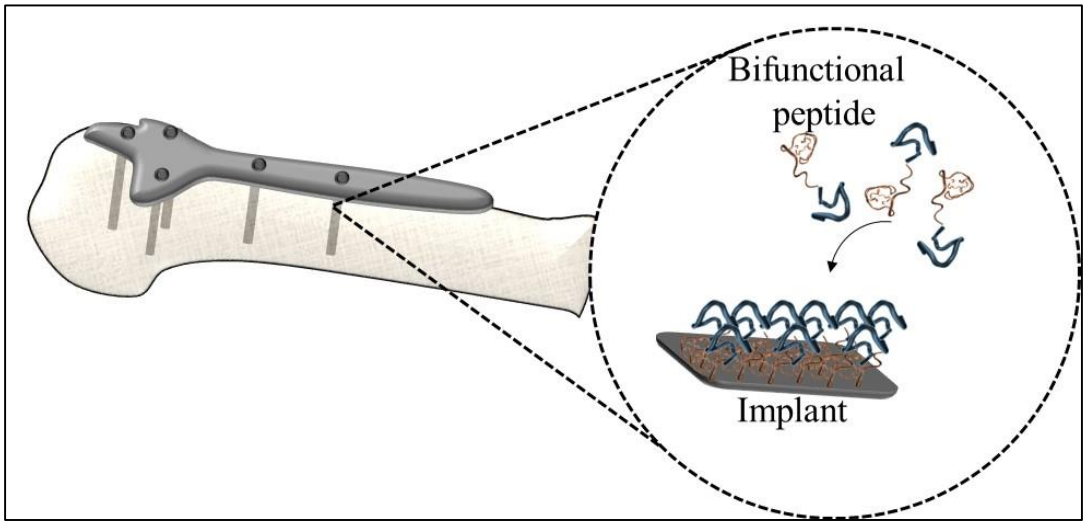

Figure 8: Schematics of peptide functionalization of titanium implant surface.

3.2.1 Selection and Characterization of Solid Binding Peptides.

The phage display technique[121] was applied on titanium grade V powder to select peptides that could serve as potential molecular linkers to tether antimicrobial peptides on implant material surfaces. Throughout the selection process, four successive rounds of biopanning were performed, resulting in 80 unique clones, which were then subjected to DNA sequence analysis. FM technique as a semi-quantitative binding assay was applied to investigate the binding affinities of individual clones. For this, each clone was incubated with titanium grade V powder and then visualized by using anti-M13 antibody and fluorophore attached secondary antibody. To evaluate the specific surface affinity of individual clones, the bound phage clones expressing titanium binding sequences were visualized as uniformly distributed bright green rods on a dark background, as opposed to wild type M13 phage, which fail to bind. Based on these results, all the identified peptides were successfully categorized as strong, moderate and weak binders (Figure 9).

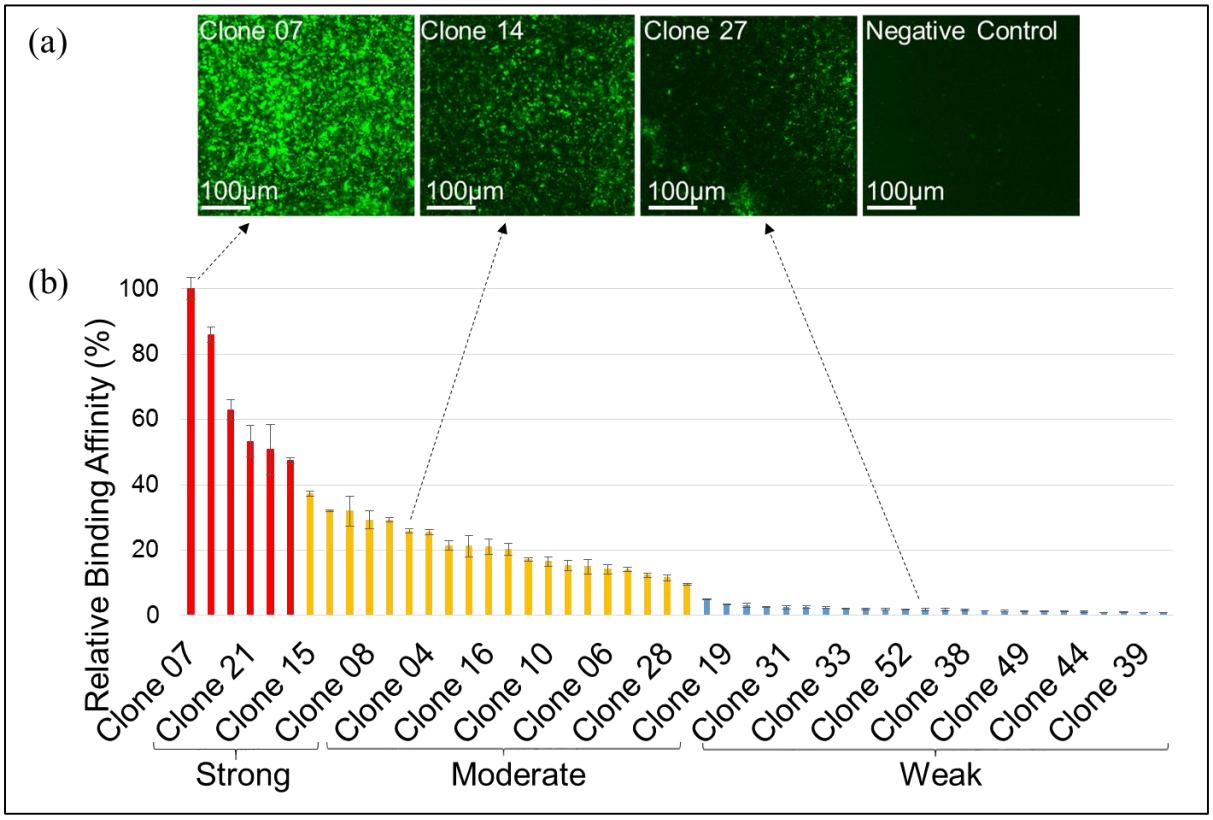

Figure 9: Titanium binding peptides (TiBP) selected by phage display: (a) examples of FM images of TiBP's with different binding affinities; (b) categorization of the titanium binding clones based on relative binding affinity analysis via FM (first two bars from left are Clone 7 and Clone 22, respectively).

To eliminate the internal bias causing from the amino acid distribution in each of phage display and cell surface display libraries , the two strongest peptides selected via phage display were further characterized and compared with titanium binding peptides that are selected by cell surface display and characterized previously.[95] Each peptides were synthesized with biotin and incubated with titanium implants. After removing the unbound peptides, surface coverage of each peptide were visualized by using fluorophore attached streptavidin probes. Based on their surface coverage ratios, peptides were categorized again (Figure 10).

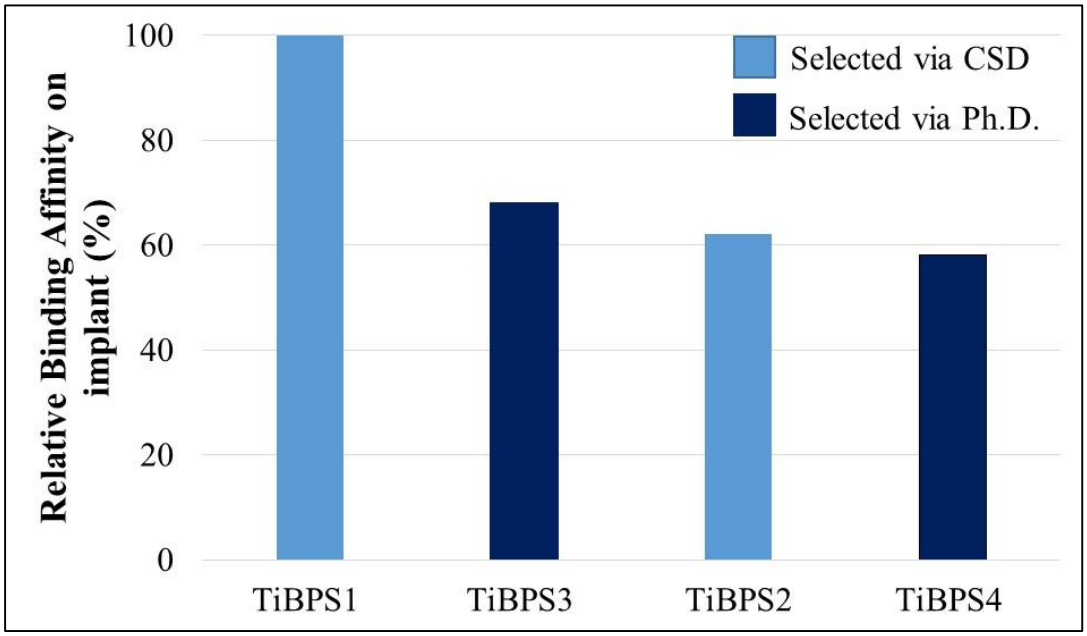

Figure 10: Relative binding affinities of titanium binding peptides (TiBP) selected by cell surface display and phage display (Phage bound TiBPS3 and TiBPS4 are represented in previous figure as Clone 7 and Clone 22, respectively.).

3.2.2 Selection and Characterization of Antimicrobial Peptides

Bacteria growth curves in the presence of antimicrobial peptides with concentrations ranging from 2 µg/mL to 512 µg/mL with two-fold increment were analyzed for a period of 24 h to determine the MIC values for the each of the bacterial strains, i.e., *S. epidermidis*, and *E. coli*, which are common for orthopedic implant infections. As shown in Table 4, AMP 1 and AMP 2 are both effective against two of these organisms yet with different MIC values. MIC values for AMP1 against *E. coli* and *S. epidermidis* are determined as 16 µg/mL and 8 µg/mL, respectively. For AMP2, MIC values against *E. coli* and *S. epidermidis* are determined as 32 µg/mL and 1 µg/mL, respectively. These concentrations indicates that the AMP1 is more effective against *E. coli* than AMP2. Whereas, AMP2 can prevent *S. epidermidis* growth with much lower concentrations than AMP1.

Table 4: Minimum inhibitory concentration (MIC) values of AMP-1 and AMP-2 against *E.coli* and *S.epidermidis*.

Peptide	Sequence	*E. coli* (µg/ml)	*S. epidermidis* (µg/ml)
AMP-1	LKLLKKLLKLLKKL	16 (9.45 µM)	8 (4.72 µM)
AMP-2	KWKRWWWWR	32 (21.08 µM)	1 (0.66 µM)

3.2.3 Construction and Characterization of Chimeric Peptides

Chimeric peptides having both titanium binding affinity and antimicrobial activity were constructed by coupling the combinatorially selected titanium binding peptides (TiBPS1, TiBPS3 and TiBPS4) with previously characterized antimicrobial peptide, i.e. AMP2 in different combinations. In this design, the biocombinatorially selected TiBP's were inserted to the C'-terminal ends of the AMP's with a structurally flexible triple glycine (GGG) linker sequence to ensure that the functionalities of neither the titanium binding peptide, nor the AMP's, were restricted by one another on the final chimeric construct. The amino acid sequences and theoretical parameters, such as MW and pI, for each chimeric peptide were listed in Table 5.

Table 5: MW, pI, net charge and the hydropathy of constructed chimeric peptides.

Peptide Name	Sequence	MW (kDa)	pI	Charge	G.R.A.V.Y score
TiBPS1-AMP2	RPRENRGRERGLGGG KWKRWWWWR	3166.6	12.13	+7	-2.254
TiBPS3-AMP2	SRPNGYGGSESSGGG KWKRWWWWR	3058.5	11.17	+5	-1.104
TiBPS4-AMP2	WSYESSTPRTQLGGG KWKRWWWWR	3125.5	11.00	+4	-1.575

Successful design of any multi-functional system requires the retention of multifunctional activities that are embedded in the final construct is confirmed. Therefore, the efficiency of the resulting chimeric peptide investigated with respect to titanium binding affinity as well as antimicrobial activity. To investigate the antimicrobial activity, chimeric peptides tested against *E. coli* and *S. epidermidis* separately, and the resulting MIC values were calculated by monitoring bacterial growth in the presence of these chimeric peptides, spectrophotometrically.

Peptide testing concentrations were chosen such that the lowest testing concentration was set to the predetermined MIC value of related AMP to be ensure that the same number of AMP present in the solution. Then, with two fold increments, rest of three higher peptide concentrations are determined.

Table 6: Minimum inhibitory concentration (MIC) values of chimeric peptides against *E.coli* and *S.epidermidis*.

Peptide Name	**Sequence**	***E. coli* (µg/ml)**	***S. epidermidis* (µg/ml)**
TiBPS1-AMP2	RPRENRGRERGLGGG KWKRWWWWR	256 (80.8 µM)	8 (2.52 µM)
TiBPS3-AMP2	SRPNGYGGSESSGGG KWKRWWWWR	512 (167.4 µM)	16 (5.23 µM)
TiBPS4-AMP2	WSYESSTPRTQLGGG KWKRWWWWR	512 (167.6 µM)	16 (5.22 µM)

As shown in Table 6, among three different chimeric peptides TiBPS1-AMP2 showed the highest antibacterial activity against *E.coli* which is 256 µg/mL (see Appendix B for details).

Furthermore, compared to the TiBPS3-AMP2 and TiBPS4-AMP2, TiBPS1-AMP2 has two times higher antimicrobial activity. The attenuation in the antimicrobial efficiency of AMP2 depending on the titanium binding peptide that is coupled can be attributed to the difference in the amino acid composition and the sequences of these chimeric peptides. In the case of *S. epidermidis*, it was revealed that the TiBPS1-AMP2 is the most effective peptide in solution by being able prevent the bacterial growth at 8 µg/mL concentration. In addition, TiBPS3-AMP2 and TiBPS4-AMP2 were

also showed a considerably good antimicrobial activity with MIC values which is about less than 16 µg/ml. The TiBPS1-AMP2 shows a two-fold reduction in the antimicrobial efficiency compared to TiBPS3-AMP2 and TiBPS4-AMP2 against both of the *E.coli* and *S. epidermidis* while the difference in binding efficiencies of titanium binding peptides are different than 2-fold. This can be attributed to the complex interactions between the bacterial cell membrane and the antimicrobial peptides during the targeting and the penetration. It also implies that overall antimicrobial activity not only depends amino acid sequence and content of the AMP, but also the membrane structure and composition of targeted microorganism. Also, the hydrophobicity of the peptide, the presence of positively charged residues, amphipatic nature of peptides, secondary structure are some of known factors that can effect both the antimicrobial activity and antimicrobial selectivity.

3.2.4 Bacterial Adhesion on Peptide Functionalized Implant Surfaces

Following to determining minimum inhibitory concentrations of each peptide against two different bacteria in solution, antimicrobial efficacy of these peptides were further characterized on the titanium implant surfaces against the most common *S.epidermidis*.

With this aim, 100 µM of each chimeric peptide were first incubated for 4 hours at 37°C with constant agitation with the pre-sterilized titanium implant surfaces. Then, the excess amount of peptide was removed by washing surface 3 times with PBS buffer. Afterwards, surfaces were incubated in bacteria culture consisting of at 10^8 cells/mL for 4 hours. After the incubation cells were fixed and labeled with SYTO 9™ dye which penetrates bacterial membranes and stains the cells green. Finally, by visualizing under fluorescence microscopy (FM), the bacterial binding and antimicrobial efficacy of peptide functionalized titanium implant surfaces were analyzed.

As a result, *S.epidermidis* adhesion on titanium implants coated with chimeric peptides was significantly reduced compared to bare titanium implant surface. As shown in figure 11, there is a 27–fold reduction in bacterial adhesion on the TiBPS3-AMP2 coated surface compared to bare surface (no peptide).

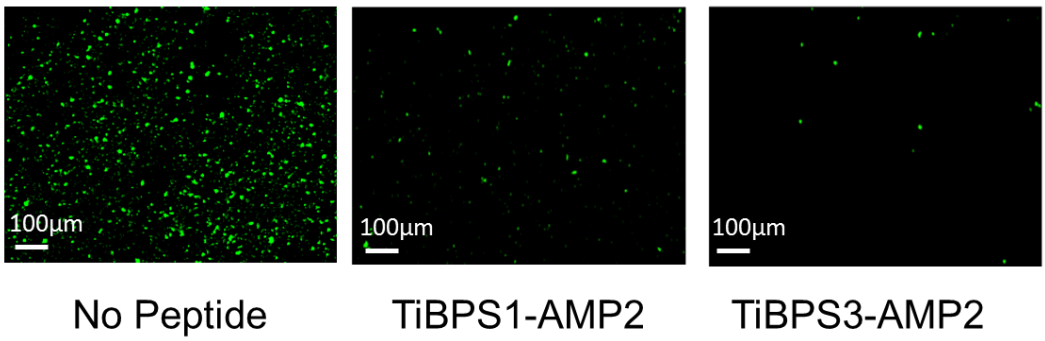

Figure 11: S. epidermidis adhesion on peptide modified titanium surfaces, i.e. no peptide (left column), TiBPS1-AMP2 (middle column), and TiBPS3-AMP2 (right column).

3.3 Case Study IIB: Tunable Bioactive Interface Design for Zirconia Based Implants

In this study, we demonstrated the use of chimeric ZrBP3-AMP1 peptide as an antimicrobial coating agent on zirconia implants (Figure 12).

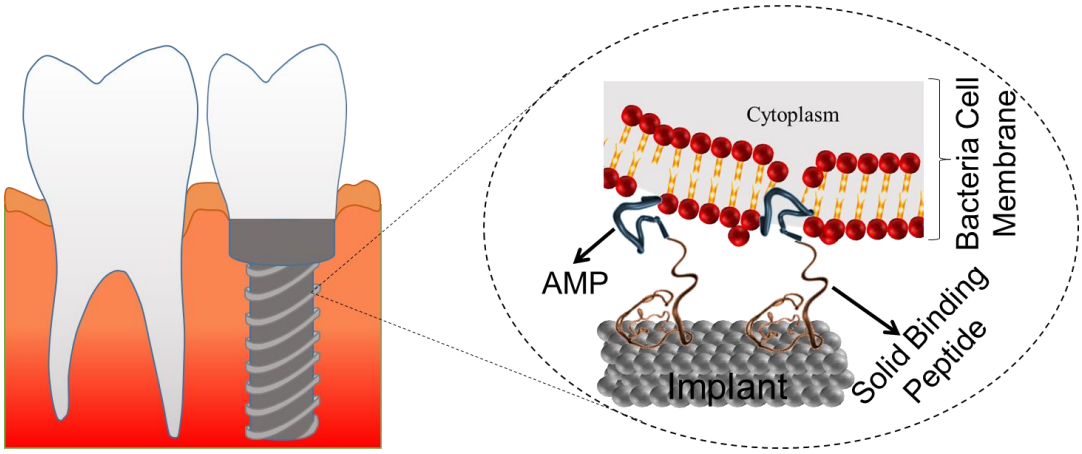

Figure 12: Schematics of peptide functionalization of zirconia implant surface.

Chimeric ZrBP3-AMP1 peptide, consisting of two functional units, i.e. a zirconia implant specific recognition and binding region and a computationally designed antimicrobial unit, was characterized in terms of its overall zirconia implant binding and coating ability as well as its antimicrobial activity against *S. mutans*, one of the most common cariogenic microorganism.

3.3.1 Selection and Characterization of Solid Binding Peptides.

In this study, zirconia binding peptide was selected using pre-constructed biotinylated peptide library comprising randomly generated different peptide sequences. First of all, each peptide was

incubated with the freshly cleaned zirconium (IV) oxide powder and then nonspecific bound peptides were removed from surface by washing steps. Surface bound peptides were then labeled with Qdot™ 605 ITK™ Streptavidin Conjugate probes and binding properties of each peptide were analyzed with respect to their substrate surface overages using FM. Among these peptides shown in figure 13, the clone 3 (ZrBP3) showed the highest surface coverage.

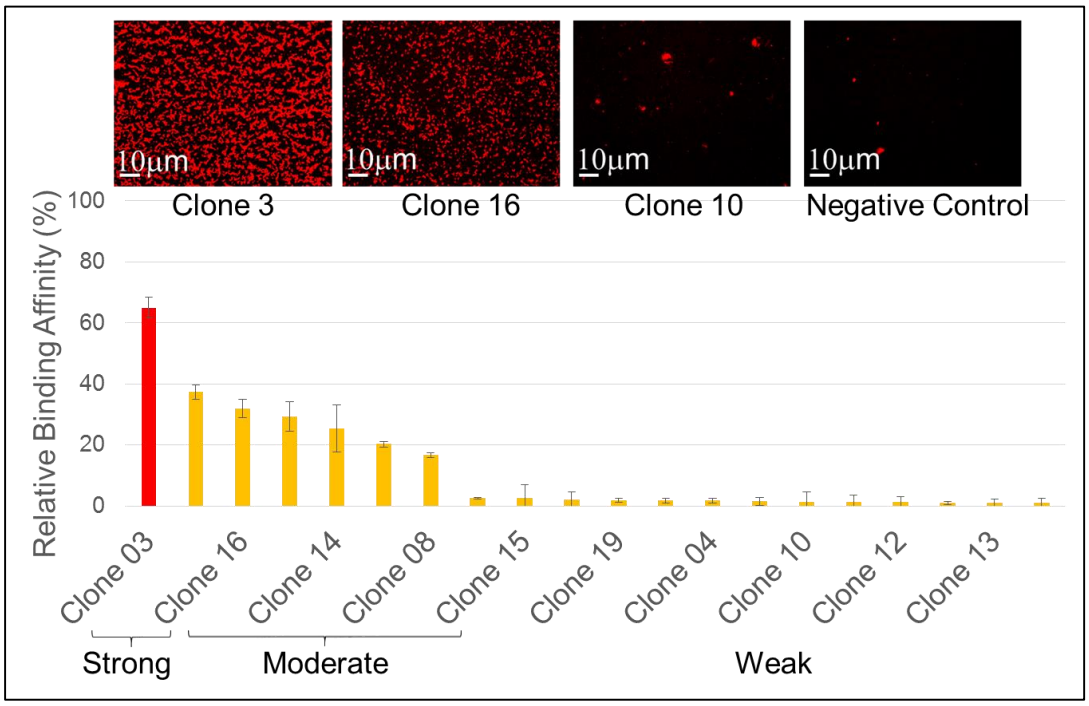

Figure 13: Relative binding affinities of selected peptides

Surface recognition and binding characteristics of peptides can be tuned through rational mutations. To enhance binding properties of experimentally selected ZrBP3 peptide, we utilized from a *de novo* method which is specifically designed for prediction of tertiary structure of small peptides and made tertiary structure predictions. Briefly, in the first step, the regular secondary structure, e.g. helix, β-strand and coil, are predicted using BetaTurns method. Next, using the Tleap module of Amber version 6, primary conformation of the peptide sequence is generated. Standard Dunbrack backbone dependent rotamer library was used to assign angles between the side chains. In the final stage, using Sander module of Amber, primary conformation of peptide was subjected to molecular dynamics simulations for energy minimization in aqueous environment at room temperature. Finally, the predicted structure was generated by minimization using a combination of steepest descent and conjugate gradient algorithms.[128]

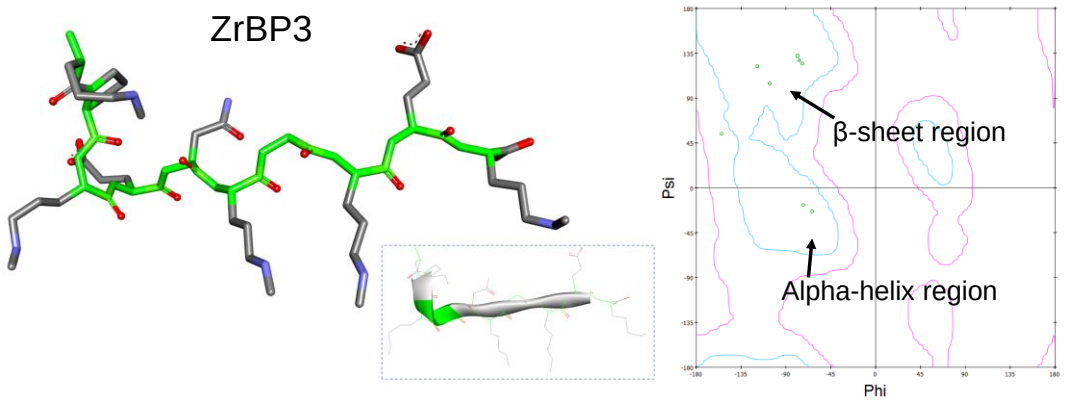

Figure 14: (a) The predicted tertiary structure and (b) the torsional distribution through the backbone of ZrBP3.

Furthermore, the Ramachandran analysis was done to plot the torsional distribution of backbone. The predicted tertiary structure and the torsional distribution through amino acids is shown in Figure 14.

As shown in Figure 14, ZrBP3 exhibits both β-sheet and alpha helix content. To enhance the binding properties of ZrBP3, we decided to increase β-sheet through amino acids of the ZrBP3 peptide single amino acid substitutions. Previous studies suggest that the charged residues in peptides make a considerable contribution to the overall binding affinity of peptides to the oxide surfaces. To be able to increase the β-sheet content of ZrBP3 peptide without changing total charge distribution, we therefore, primarily targeted the charge neutral asparagine residue (5^{th} amino acid) on ZrBP3 peptide and substituted it with another neutral glutamine which has a similar hydrophobicity yet longer side group. As shown in Figure 15, the overall β-sheet content through backbone of the peptide with glutamine substitution (ZrBP3-M1) was increased compared to ZrBP3. More importantly, this substitution mutation led to a more linear tertiary structure.

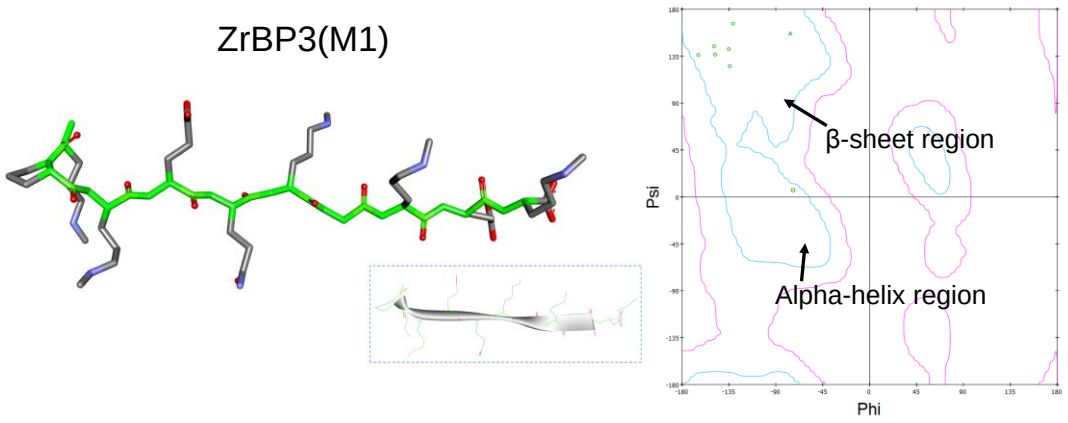

Figure 15: (a) The predicted tertiary structure and (b) the torsional distribution through the backbone of ZrBP3_M1.

In the next step, both of the ZrBP3 and ZrBP3(M1) peptides were synthesized with biotin on their N-terminal ends and their binding efficacies were experimentally characterized on zirconia implant grade disks using Qdot™ 605 ITK™ Streptavidin probes under FM. Interestingly, both peptides showed similar surface coverages on zirconia implant grade disks. As expected, ZrBP3(M1) showed a 10 % enhancement in surface coverage compared to ZrBP3 suggesting that the increase in the β-sheet content positively effects the binding properties ZrBP3.

3.3.2 Selection and Characterization of Antimicrobial Peptides

Minimum inhibition concentration (MIC) of antimicrobial peptides that are selected from literature (see section 3.2.2) were determined against *S. mutans* and *E. coli*. For this, bacteria growth in freshly inoculated culture was monitored in the presence of AMP1 with different concentrations ranging from 8 µg/mL to 256 µg/mL for a period of 24 h. As shown in Table 7, AMP 1 effective MIC against *S. mutans* in solution is 64 µg/mL.

Table 7: Minimum inhibitory concentration (MIC) values of AMP-1 against *E.coli* and *S.mutans*.

Peptide	**Sequence**	***E. coli* (µg/ml)**	***S. mutans* (µg/ml)**
AMP-1	LKLLKKLLKLLKKL	16 (9.45 µM)	64 (37.81 µM)

3.3.3 Construction and Characterization of Chimeric Peptides

After selection and characterization of the zirconia binding peptide and antimicrobial peptides separately, in the next step we have constructed the bifunctional/chimeric peptides. To do this, we used the same approach that is described in Section 3.2.3.

Targeting and disrupting the integrity of negatively charged cell membranes of microorganisms is the one of the main reaction mechanism of antimicrobial peptides. Therefore, it is very important to maintain its mobility and accessibility on the constructed the chimeric peptide. To maintain in solution antimicrobial properties of AMP1 on the surface, a structurally flexible triple glycine (GGG) linker sequence utilized in between zirconia binding peptides and the antimicrobial peptide (AMP1). This way we ensured that neither the binding properties of ZrBP's nor the antimicrobial characteristics of AMP negatively affected due to the restriction of one peptide to another on the final product.

The full length amino acid sequences and theoretical parameters, such as MW and pI, for constructed chimeric peptide were listed in Table 8, below.

Table 8: MW, pI, net charge and the hydropathy of constructed chimeric peptides.

Peptide Name	Sequence	MW (kDa)	pI	Charge	G.R.A.V.Y score
ZrBP3-AMP1	RPRENRGRERGGG LKLLKKLLKLLKKL	3170.9	11.85	+9	-1.081
ZrBP3(M1)-AMP1	RPREQRGRERGGG LKLLKKLLKLLKKL	3184.9	11.85	+9	-1.081

The constructed chimeric peptides were initially tested to determine their antimicrobial properties in the solution state. The antimicrobial activities of each peptide were tested using the methods described above (see section 3.2.2) for both *E. coli* and *S. mutans* bacterial strains and the spectrophotometrically calculated MICs are reported in Table 9 below.

Table 9: Minimum inhibitory concentration (MIC) values of chimeric peptides against *E.coli* and *S. mutans*.

Peptide Name	Sequence	MW (kDa)	pI	Charge	G.R.A.V.Y score
ZrBP3-AMP1	RPRENRGRERGGG LKLLKKLLKLLKKL	3170.9	11.85	+9	-1.081
ZrBP3(M1)-AMP1	RPREQRGRERGGG LKLLKKLLKLLKKL	3184.9	11.85	+9	-1.081

As shown in Table 9, both peptides showed similar in solution antimicrobial activities against *E.coli* and *S. mutans* which are 32 µg/mL 256 µg/mL, respectively (see Appendix C for details). Although both peptides (ZrBP3 (M1)-AMP1 and ZrBP3-AMP1) were active against both bacterial strains, the MIC values was 2 times greater than that for AMP1 alone against *S. mutans*; which can likely be explained by the presence of the additional 10 amino acid residues contained in the N'-terminal end of the peptide. Furthermore, the 2 fold increase in MIC values can also be explained with the change on the overall charge distribution of the peptide due to the presence of 10 extra amino acid residues on peptide.

3.3.4 Bacterial Adhesion on Peptide Functionalized Implant Surfaces

Although in solution MIC values are useful predictors for antimicrobial efficacy of peptides, these measurements do not directly correlate to on surface antimicrobial activities immobilized peptides due to the differential diffusion and molecular recognition mechanisms between inorganic surface and peptide as well as the complex supra-molecular interactions between peptides. Therefore in the next step, the bacterial attachment on peptide coated zirconia disc implants were performed by exposing the surfaces to bacteria suspension and monitoring the level of cellular attachment.

For this analysis, 100 µM of each chimeric peptide were first incubated the 4 hours at 37°C with constant agitation with the pre-cleaned zirconia disc implants. Then, the excess amount of peptide was removed by washing surface 3 times with PBS buffer. Then, surfaces were soaked into bacteria culture consisting of at 10^8 cells/mL for 4 hours. To remove unattached and/or weakly attached bacterial cells, surfaces were washed again with 1X PBS buffer. The adhering cells were then fixed and labeled with SYTO 9™ dye and subjected to FM analysis.

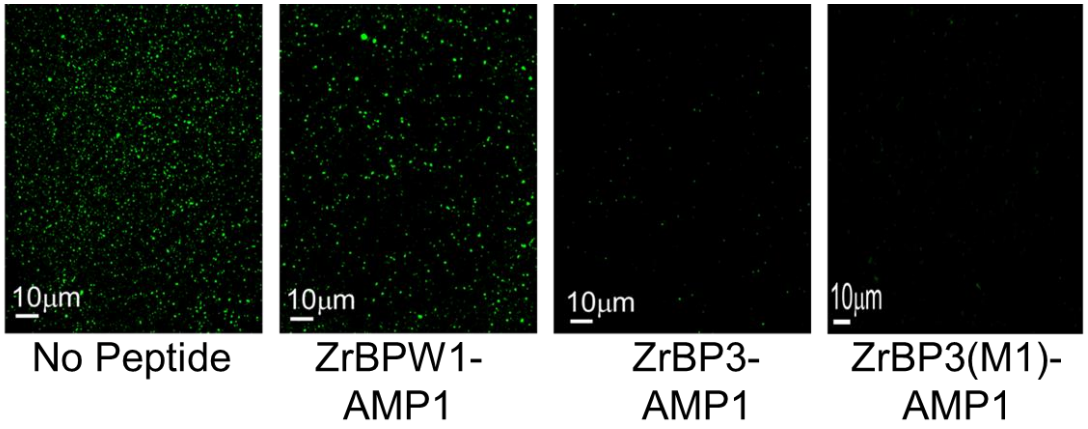

Figure 16: *S. mutans* adhesion on peptide modified zirconia surfaces, i.e. no peptide (left column), ZrBPW3-AMP1 (middle left column), and ZrBPS3-AMP1 (middle right column), ZrBPS3_M1-AMP1 (right column)

As expected, *S.mutans* attachment on peptide coated surfaces were significantly reduced compared to the bare surfaces. As shown in Figure 16, there is a 90- and 50- fold reduction in bacterial adhesion on the ZrBP3(M1)-AMP1 and ZrBP3-AMP1 coated surface compared to bare surface (no peptide), respectively. Compared with ZrBP3(M1)-AMP1, increased bacterial attachment to ZrBP3-AMP1 coated surfaces could be explained either by difference between the substrate binding properties of zirconia binding counterparts of chimeric peptide, or by the effect of amino acid substitution over the assembly density of chimeric peptides.

4. Conclusion

With three case studies, we have demonstrated the functional utility of GEPI as an anchoring molecule as well as biological surface functionalizer. Our case studies demonstrates that solid binding peptides can be applied as an anchoring molecule either genetically engineered to couple with an enzyme resulting in single step immobilization with orientation control or as synthesized using solid state chemistry to couple bioactivity to the medical grade implant surfaces.

The case study I describes genetically engineering a dehydrogenase to form a self-organized enzyme integrated circuit based sensor. Our approach is composed of three steps, i) designing an engineered protein, which features an FDH catalytic unit from *Candida methylica* and a highly specific gold-binding peptide (AuBP2) as a genetically conjugated tag that enables direct assembly of the enzyme onto a gold surface, ii) the corroboration of the chimeric activities in the system by applying biochemical as well as surface binding assays, iii) designing a circuit based sensor system that is integrated with the self-organized engineered enzyme where the catalytic conversion of the formate can be monitored by the subsequence generation of electrons as an output in the current.

The developed peptide based design incorporates different novelties that are built upon bridging genetic engineering to solid material interfaces to develop controlled bio-material interfacial interactions. First, a structurally flexible spacer sequence is integrated as an engineering design parameter to keep the protein's distinct functionalities not to be restricted by additional domain. Second, a novel cleavage site was introduced to allow removing purification tag to investigate the peptide as the sole effect on surface functionalization. A single step assembly of the enzyme was achieved within a close proximity which enabled to design a circuit-based electrode system. The redox catalysis ability of the self-immobilized enzyme on gold electrode was verified by subsequent addition of formate and prolonged consequent current generation. The proposed engineered fusion enzyme based platform can be used for monitoring a wide range of industrial applications, e.g. formate detection in agrochemical industries or NADH regeneration from NAD^+ in pharmaceutical research and development sectors.

Functional proteins genetically coupled with material specific peptide tags offer a simple single-step, bio-friendly alternative to the conventional chemical and physical immobilization methods, without the requirement of undesired surface activation processes. The proposed immobilization strategy is a step toward achieving self-integrated enzyme harboring platforms and may lead to the improvement of sensing and fuel cell devices in the future.

In case study IIA and IIB, the surface functionalization ability of GEPI in the form of chimeric peptide design was shown. In case study IIB and IIB, we describe a peptide-based implant surface functionalization approach to prevent bacterial infections derived implant failure. Chimeric peptides having specific surface recognition and binding ability as well as antimicrobial activity were designed and synthesized by solid phase peptide synthesis. Then, the original titanium alloy (case study IIA) zirconia (case study IIB) implant surfaces were first self-coated with these peptides and then the coated implant surfaces were subjected to bacteria culture to test bacterial growth and/or adhesion on implant. In solution activity tests revealed that the antimicrobial functionality of the peptides is conserved in the bifunctional form. Furthermore, the bacterial adhesion studies demonstrated that both implants (titanium alloy (case study IIA) zirconia (case study IIB)) are gained antimicrobial functionality through chimeric peptide coating. Our findings demonstrated that the interfacial antimicrobial peptide coating significantly reduced the bacterial colonization and thereby, gained an antimicrobial functionality to the implants.

Collectively, the effective use of solid binding peptides were demonstrated to integrate the desired bioactivity to the surfaces, i.e. antimicrobial peptides as enablers to induce control at the tissue-implant interface. This is very critical not only to promote healthy tissue growth but also to prevent implant failure that are caused by infections. More importantly, solid-binding peptides offer a single-step, bio-friendly alternative to the conventional chemical and physical immobilization methods, without the requirement of surface activation processes that are consists of multiple steps. In conclusion, as a molecular tool, GEPI can be used as anchoring and surface functionalization molecule as well as a molecular linker combining different functions. The strategy developed here can be applied to a wide range of practical applications by combining multiple biological units having diverse functions.

5. Future Work

Objectives for future work include the development of a superior multi-enzyme harboring biosensing systems to more enhance the accuracy and sensitivity.

For case study IIA and IIB, future work includes the evaluation of the *in vivo* and *in vitro* cytotoxicity of developed chimeric peptides. Furthermore, surface coverage and antimicrobial efficacy chimeric peptides can be further enhanced by designing a robust carrier peptides. Moreover, co-assembly of antifouling peptides with the developed antimicrobial chimeric peptides can lead to improve the surface properties of implant materials.

6. References

1. Patolsky, F.; Timko, B. P.; Zheng, G.; Lieber, C. M. Nanowire-based nanoelectronic devices in the life sciences. MRS bulletin 2007, 32, 142-149.
2. Elnathan, R.; Kwiat, M.; Pevzner, A., et al. Biorecognition layer engineering: overcoming screening limitations of nanowire-based FET devices. Nano letters 2012, 12, 5245-5254.
3. Sassolas, A.; Blum, L. J.; Leca-Bouvier, B. D. Immobilization strategies to develop enzymatic biosensors. Biotechnology advances 2012, 30, 489-511.
4. Katz, E.; MacVittie, K. Implanted biofuel cells operating in vivo–methods, applications and perspectives–feature article. Energy & Environmental Science 2013, 6, 2791-2803.
5. Katz, E.; Minko, S.; Halámek, J.; MacVittie, K.; Yancey, K. Electrode interfaces switchable by physical and chemical signals for biosensing, biofuel, and biocomputing applications. Analytical and bioanalytical chemistry 2013, 405, 3659-3672.
6. Asanomi, Y.; Yamaguchi, H.; Miyazaki, M.; Maeda, H. Enzyme-immobilized microfluidic process reactors. Molecules 2011, 16, 6041-6059.
7. Cetinel, S.; Dincer, S.; Cebeci, A., et al. Peptides to bridge biological-platinum materials interface. Bioinspired, Biomimetic and Nanobiomaterials 2012, 1, 143-153.
8. Hnilova, M.; Karaca, B. T.; Park, J., et al. Fabrication of hierarchical hybrid structures using bio-enabled layer-by-layer self-assembly. Biotechnology and bioengineering 2012, 109, 1120-1130.
9. Fuentes, M.; Pessela, B. C.; Maquiese, J. V., et al. Reversible and Strong Immobilization of Proteins by Ionic Exchange on Supports Coated with Sulfate-Dextran. Biotechnology progress 2004, 20, 1134-1139.
10. Piletsky, S.; Piletska, E.; Bossi, A.; Turner, N.; Turner, A. Surface functionalization of porous polypropylene membranes with polyaniline for protein immobilization. Biotechnology and bioengineering 2003, 82, 86-92.
11. Yam, C. M.; Deluge, M.; Tang, D.; Kumar, A.; Cai, C. Preparation, characterization, resistance to protein adsorption, and specific avidin–biotin binding of poly (amidoamine) dendrimers functionalized with oligo (ethylene glycol) on gold. Journal of colloid and interface science 2006, 296, 118-130.

12. Viitala, T.; Vikholm, I.; Peltonen, J. Protein immobilization to a partially cross-linked organic monolayer. Langmuir 2000, 16, 4953-4961.
13. Mendes, R.; Carvalhal, R.; Kubota, L. Effects of different self-assembled monolayers on enzyme immobilization procedures in peroxidase-based biosensor development. Journal of Electroanalytical Chemistry 2008, 612, 164-172.
14. Masri, M. S.; Friedman, M. Protein reactions with methyl and ethyl vinyl sulfones. Journal of protein chemistry 1988, 7, 49-54.
15. Rusmini, F.; Zhong, Z.; Feijen, J. Protein immobilization strategies for protein biochips. Biomacromolecules 2007, 8, 1775-1789.
16. Jongsma, M. A.; Litjens, R. H. Self-assembling protein arrays on DNA chips by auto-labeling fusion proteins with a single DNA address. Proteomics 2006, 6, 2650-2655.
17. Gauvreau, V.; Chevallier, P.; Vallières, K.; Petitclerc, É.; Gaudreault, R. C.; Laroche, G. Engineering surfaces for bioconjugation: developing strategies and quantifying the extent of the reactions. Bioconjugate chemistry 2004, 15, 1146-1156.
18. Lee, K.-B.; Park, S.-J.; Mirkin, C. A.; Smith, J. C.; Mrksich, M. Protein nanoarrays generated by dip-pen nanolithography. Science 2002, 295, 1702-1705.
19. Marcus, R. A.; Sutin, N. Electron transfers in chemistry and biology. Biochimica et Biophysica Acta (BBA)-Reviews on Bioenergetics 1985, 811, 265-322.
20. Kuila, T.; Bose, S.; Khanra, P.; Mishra, A. K.; Kim, N. H.; Lee, J. H. Recent advances in graphene-based biosensors. Biosensors and Bioelectronics 2011, 26, 4637-4648.
21. Shao, Y.; Wang, J.; Wu, H.; Liu, J.; Aksay, I. A.; Lin, Y. Graphene based electrochemical sensors and biosensors: a review. Electroanalysis 2010, 22, 1027-1036.
22. Krauland, E. M.; Peelle, B. R.; Wittrup, K. D.; Belcher, A. M. Peptide tags for enhanced cellular and protein adhesion to single-crystalline sapphire. Biotechnology and bioengineering 2007, 97, 1009-1020.
23. Sarikaya, M.; Tamerler, C.; Jen, A. K.-Y.; Schulten, K.; Baneyx, F. Molecular biomimetics: nanotechnology through biology. Nature materials 2003, 2, 577-585.
24. Whaley, S. R.; English, D.; Hu, E. L.; Barbara, P. F.; Belcher, A. M. Selection of peptides with semiconductor binding specificity for directed nanocrystal assembly. Nature 2000, 405, 665-668.

25. Tamerler, C.; Khatayevich, D.; Gungormus, M., et al. Molecular Biomimetics: GEPI-Based Biological Routes to Technology. Biopolymers 2010, 94, 78-94.
26. Naik, R. R.; Stringer, S. J.; Agarwal, G.; Jones, S. E.; Stone, M. O. Biomimetic synthesis and patterning of silver nanoparticles. Nature materials 2002, 1, 169-172.
27. Kacar, T.; Zin, M. T.; So, C., et al. Directed self-immobilization of alkaline phosphatase on micro-patterned substrates via genetically fused metal-binding peptide. Biotechnology and bioengineering 2009, 103, 696-705.
28. Khatayevich, D.; Gungormus, M.; Yazici, H., et al. Biofunctionalization of materials for implants using engineered peptides. Acta biomaterialia 2010, 6, 4634-4641.
29. Puddu, V.; Perry, C. C. Peptide adsorption on silica nanoparticles: evidence of hydrophobic interactions. ACS nano 2012, 6, 6356-6363.
30. Notman, R.; Walsh, T. R. Molecular dynamics studies of the interactions of water and amino acid analogues with quartz surfaces. Langmuir 2009, 25, 1638-1644.
31. Dai, H.; Choe, W.-S.; Thai, C. K., et al. Nonequilibrium synthesis and assembly of hybrid inorganic-protein nanostructures using an engineered DNA binding protein. Journal of the American Chemical Society 2005, 127, 15637-15643.
32. Sengupta, A.; Thai, C. K.; Sastry, M., et al. A genetic approach for controlling the binding and orientation of proteins on nanoparticles. Langmuir 2008, 24, 2000-2008.
33. Cetinel, S.; Caliskan, H. B.; Yucesoy, D. T., et al. Addressable self-immobilization of lactate dehydrogenase across multiple length scales. Biotechnology journal 2013, 8, 262-272.
34. Hnilova, M.; Liu, X.; Yuca, E., et al. Multifunctional protein-enabled patterning on arrayed ferroelectric materials. ACS applied materials & interfaces 2012, 4, 1865-1871.
35. Yuca, E.; Karatas, A. Y.; Seker, U. O. S., et al. In vitro labeling of hydroxyapatite minerals by an engineered protein. Biotechnology and bioengineering 2011, 108, 1021-1030.
36. Liu, W.; Wang, P. Cofactor regeneration for sustainable enzymatic biosynthesis. Biotechnology advances 2007, 25, 369-384.
37. Hummel, W. Large-scale applications of NAD (P)-dependent oxidoreductases: recent developments. Trends in biotechnology 1999, 17, 487-492.
38. Tishkov, V. I.; Popov, V. O. Protein engineering of formate dehydrogenase. Biomolecular engineering 2006, 23, 89-110.

39. Kratzer, R.; Pukl, M.; Egger, S.; Nidetzky, B. Whole-cell bioreduction of aromatic α-keto esters using Candida tenuis xylose reductase and Candida boidinii formate dehydrogenase co-expressed in Escherichia coli. Microbial Cell Factories 2008, 7, 37-48.
40. Karagüler, N.; Sessions, R.; Binay, B.; Ordu, E.; Clarke, A. Protein engineering applications of industrially exploitable enzymes: Geobacillus stearothermophilus LDH and Candida methylica FDH. Biochemical Society Transactions 2007, 35, 1610-1615.
41. Reda, T.; Plugge, C. M.; Abram, N. J.; Hirst, J. Reversible interconversion of carbon dioxide and formate by an electroactive enzyme. Proceedings of the National Academy of Sciences 2008, 105, 10654-10658.
42. Roche, J.; Groenen-Serrano, K.; Reynes, O.; Chauvet, F.; Tzedakis, T. NADH regenerated using immobilized FDH in a continuously supplied reactor–Application to l-lactate synthesis. Chemical Engineering Journal 2014, 239, 216-225.
43. Bolivar, J. M.; Wilson, L.; Ferrarotti, S. A.; Fernandez-Lafuente, R.; Guisan, J. M.; Mateo, C. Evaluation of different immobilization strategies to prepare an industrial biocatalyst of formate dehydrogenase from Candida boidinii. Enzyme and microbial technology 2007, 40, 540-546.
44. Addo, P. K.; Arechederra, R. L.; Minteer, S. D. Evaluating Enzyme Cascades for Methanol/Air Biofuel Cells Based on NAD+-Dependent Enzymes. Electroanalysis 2010, 22, 807-812.
45. Allen, S.; Holbrook, J. Isolation, sequence and overexpression of the gene encoding NAD-dependent formate dehydrogenase from the methylotrophic yeast Candida methylica. Gene 1995, 162, 99-104.
46. Ordu, E. B.; Karagüler, N. G. Improving the Purification of NAD+-Dependent Formate Dehydrogenase from Candida methylica. Preparative Biochemistry and Biotechnology 2007, 37, 333-341.
47. Bauer, S.; Schmuki, P.; von der Mark, K.; Park, J. Engineering biocompatible implant surfaces: Part I: Materials and surfaces. Progress in Materials Science 2013, 58, 261-326.
48. Puleo, D.; Nanci, A. Understanding and controlling the bone–implant interface. Biomaterials 1999, 20, 2311-2321.
49. Geetha, M.; Singh, A.; Asokamani, R.; Gogia, A. Ti based biomaterials, the ultimate choice for orthopaedic implants–a review. Progress in Materials Science 2009, 54, 397-425.

50. Le Guéhennec, L.; Soueidan, A.; Layrolle, P.; Amouriq, Y. Surface treatments of titanium dental implants for rapid osseointegration. Dental materials 2007, 23, 844-854.
51. Pennekamp, P. H.; Gessmann, J.; Diedrich, O., et al. Short-term microvascular response of striated muscle to cp-Ti, Ti-6Al-4V, and Ti-6Al-7Nb. Journal of orthopaedic research 2006, 24, 531-540.
52. Costerton, J.; Stewart, P. S.; Greenberg, E. Bacterial biofilms: a common cause of persistent infections. Science 1999, 284, 1318-1322.
53. Weinstein, R. A.; Darouiche, R. O. Device-associated infections: a macroproblem that starts with microadherence. Clinical Infectious Diseases 2001, 33, 1567-1572.
54. Uçkay, I.; Hoffmeyer, P.; Lew, D.; Pittet, D. Prevention of surgical site infections in orthopaedic surgery and bone trauma: state-of-the-art update. Journal of Hospital Infection 2013, 84, 5-12.
55. Antoci Jr, V.; Adams, C. S.; Parvizi, J., et al. The inhibition of Staphylococcus epidermidis biofilm formation by vancomycin-modified titanium alloy and implications for the treatment of periprosthetic infection. Biomaterials 2008, 29, 4684-4690.
56. Kazemzadeh-Narbat, M.; Kindrachuk, J.; Duan, K.; Jenssen, H.; Hancock, R. E.; Wang, R. Antimicrobial peptides on calcium phosphate-coated titanium for the prevention of implant-associated infections. Biomaterials 2010, 31, 9519-9526.
57. Rathbone, C. R.; Cross, J. D.; Brown, K. V.; Murray, C. K.; Wenke, J. C. Effect of various concentrations of antibiotics on osteogenic cell viability and activity. Journal of Orthopaedic Research 2011, 29, 1070-1074.
58. Hetrick, E. M.; Schoenfisch, M. H. Reducing implant-related infections: active release strategies. Chemical Society Reviews 2006, 35, 780-789.
59. Campoccia, D.; Montanaro, L.; Speziale, P.; Arciola, C. R. Antibiotic-loaded biomaterials and the risks for the spread of antibiotic resistance following their prophylactic and therapeutic clinical use. Biomaterials 2010, 31, 6363-6377.
60. Harbers, G. M.; Emoto, K.; Greef, C., et al. Functionalized poly (ethylene glycol)-based bioassay surface chemistry that facilitates bio-immobilization and inhibits nonspecific protein, bacterial, and mammalian cell adhesion. Chemistry of Materials 2007, 19, 4405-4414.

61. Shimotoyodome, A.; Koudate, T.; Kobayashi, H., et al. Reduction of Streptococcus mutans adherence and dental biofilm formation by surface treatment with phosphorylated polyethylene glycol. Antimicrobial agents and chemotherapy 2007, 51, 3634-3641.
62. An, Y.; Stuart, G.; McDowell, S.; McDaniel, S.; Kang, Q.; Friedman, R. Prevention of bacterial adherence to implant surfaces with a crosslinked albumin coating in vitro. Journal of orthopaedic research 1996, 14, 846-849.
63. Jose, B.; Antoci Jr, V.; Zeiger, A. R.; Wickstrom, E.; Hickok, N. J. Vancomycin Covalently Bonded to Titanium Beads Kills Staphylococcus aureus. Chemistry & biology 2005, 12, 1041-1048.
64. Price, J.; Tencer, A.; Arm, D.; Bohach, G. Controlled release of antibiotics from coated orthopedic implants. Journal of biomedical materials research 1996, 30, 281-286.
65. Russell, A.; Tattawasart, U.; Maillard, J.-Y.; Furr, J. Possible link between bacterial resistance and use of antibiotics and biocides. Antimicrobial agents and chemotherapy 1998, 42, 2151-2151.
66. Wininger, D. A.; Fass, R. J. Antibiotic-impregnated cement and beads for orthopedic infections. Antimicrobial agents and chemotherapy 1996, 40, 2675-2679.
67. Harris, L.; Mead, L.; Müller-Oberländer, E.; Richards, R. Bacteria and cell cytocompatibility studies on coated medical grade titanium surfaces. Journal of Biomedical Materials Research Part A 2006, 78, 50-58.
68. Banerjee, I.; Pangule, R. C.; Kane, R. S. Antifouling Coatings: Recent Developments in the Design of Surfaces That Prevent Fouling by Proteins, Bacteria, and Marine Organisms. Advanced Materials 2011, 23, 690-718.
69. Zhao, L. Z.; Chu, P. K.; Zhang, Y. M.; Wu, Z. F. Antibacterial Coatings on Titanium Implants. Journal of Biomedical Materials Research Part B: Applied Biomaterials 2009, 91B, 470-480.
70. Gottenbos, B.; van der Mei, H. C.; Klatter, F.; Nieuwenhuis, P.; Busscher, H. J. In vitro and in vivo antimicrobial activity of covalently coupled quaternary ammonium silane coatings on silicone rubber. Biomaterials 2002, 23, 1417-1423.
71. Mrksich, M.; Whitesides, G. M. Using self-assembled monolayers to understand the interactions of man-made surfaces with proteins and cells. Annual review of biophysics and biomolecular structure 1996, 25, 55-78.

72. Mohorcic, M.; Jerman, I.; Zorko, M., et al. Surface with antimicrobial activity obtained through silane coating with covalently bound polymyxin B. Journal of Materials Science: Materials in Medicine 2010, 21, 2775-2782.
73. Love, J. C.; Estroff, L. A.; Kriebel, J. K.; Nuzzo, R. G.; Whitesides, G. M. Self-assembled monolayers of thiolates on metals as a form of nanotechnology. Chemical reviews 2005, 105, 1103-1169.
74. Harris, L. G.; Richards, R. G. Staphylococci and implant surfaces: a review. Injury 2006, 37, 3-14.
75. Brogden, K. A. Antimicrobial peptides: pore formers or metabolic inhibitors in bacteria? Nature Reviews Microbiology 2005, 3, 238-250.
76. Giuliani, A.; Pirri, G.; Nicoletto, S. F. Antimicrobial peptides: an overview of a promising class of therapeutics. Central European Journal of Biology 2007, 2, 1-33.
77. Zasloff, M. Antimicrobial peptides of multicellular organisms. Nature 2002, 415, 389-395.
78. Reddy, K.; Yedery, R.; Aranha, C. Antimicrobial peptides: premises and promises. International journal of antimicrobial agents 2004, 24, 536-547.
79. Pasupuleti, M.; Schmidtchen, A.; Malmsten, M. Antimicrobial peptides: key components of the innate immune system. Critical reviews in biotechnology 2012, 32, 143-171.
80. Jenssen, H.; Hamill, P.; Hancock, R. E. Peptide antimicrobial agents. Clinical microbiology reviews 2006, 19, 491-511.
81. Ingham, A. B.; Moore, R. J. Recombinant production of antimicrobial peptides in heterologous microbial systems. Biotechnology and applied biochemistry 2007, 47, 1-9.
82. Hilpert, K.; Elliott, M. R.; Volkmer-Engert, R., et al. Sequence requirements and an optimization strategy for short antimicrobial peptides. Chemistry & Biology 2006, 13, 1101-1107.
83. Fjell, C. D.; Jenssen, H.; Hilpert, K., et al. Identification of Novel Antibacterial Peptides by Chemoinformatics and Machine Learning. Journal of medicinal chemistry 2009, 52, 2006-2015.
84. Jiang, Z. Q.; Vasil, A. I.; Hale, J. D.; Hancock, R. E. W.; Vasil, M. L.; Hodges, R. S. Effects of net charge and the number of positively charged residues on the biological activity of amphipathic alpha-helical cationic antimicrobial peptides. Biopolymers 2008, 90, 369-383.

85. Campoccia, D.; Montanaro, L.; Arciola, C. R. A review of the biomaterials technologies for infection-resistant surfaces. Biomaterials 2013, 34, 8533-8554.
86. Kwakman, P. H. S.; Velde, A. A. T.; Vandenbroucke-Grauls, C. M. J. E.; Van Deventer, S. J. H.; Zaat, S. A. J. Treatment and prevention of Staphylococcus epidermidis experimental biomaterial-associated infection by bactericidal peptide 2. Antimicrobial Agents and Chemotherapy 2006, 50, 3977-3983.
87. Etienne, O.; Picart, C.; Taddei, C., et al. Multilayer polyelectrolyte films functionalized by insertion of defensin: A new approach to protection of implants from bacterial colonization. Antimicrobial Agents and Chemotherapy 2004, 48, 3662-3669.
88. Appendini, P.; Hotchkiss, J. H. Surface modification of poly(styrene) by the attachment of an antimicrobial peptide. Journal of applied polymer science 2001, 81, 609-616.
89. Puckett, S. D.; Taylor, E.; Raimondo, T.; Webster, T. J. The relationship between the nanostructure of titanium surfaces and bacterial attachment. Biomaterials 2010, 31, 706-713.
90. Campoccia, D.; Montanaro, L.; Arciola, C. R. The significance of infection related to orthopedic devices and issues of antibiotic resistance. Biomaterials 2006, 27, 2331-2339.
91. Costa, F.; Carvalho, I. F.; Montelaro, R. C.; Gomes, P.; Martins, M. C. L. Covalent immobilization of antimicrobial peptides (AMPs) onto biomaterial surfaces. Acta Biomaterialia 2011, 7, 1431-1440.
92. Meyers, S. R.; Khoo, X. J.; Huang, X.; Walsh, E. B.; Grinstaff, M. W.; Kenan, D. J. The development of peptide-based interfacial biomaterials for generating biological functionality on the surface of bioinert materials. Biomaterials 2009, 30, 277-286.
93. Yoshinari, M.; Kato, T.; Matsuzaka, K.; Hayakawa, T.; Shiba, K. Prevention of biofilm formation on titanium surfaces modified with conjugated molecules comprised of antimicrobial and titanium-binding peptides. Biofouling 2010, 26, 103-110.
94. Yazici, H.; Fong, H.; Wilson, B., et al. Biological response on a titanium implant-grade surface functionalized with modular peptides. Acta Biomaterialia 2013, 9, 5341-5352.
95. Denry, I.; Kelly, J. R. State of the art of zirconia for dental applications. Dental materials 2008, 24, 299-307.
96. Pjetursson, B. E.; Brägger, U.; Lang, N. P.; Zwahlen, M. Comparison of survival and complication rates of tooth-supported fixed dental prostheses (FDPs) and implant-supported FDPs and single crowns (SCs). Clinical Oral Implants Research 2007, 18, 97-113.

97. Andreiotelli, M.; Wenz, H. J.; Kohal, R. J. Are ceramic implants a viable alternative to titanium implants? A systematic literature review. Clinical Oral Implants Research 2009, 20, 32-47.
98. Rimondini, L.; Cerroni, L.; Carrassi, A.; Torricelli, P. Bacterial colonization of zirconia ceramic surfaces: an in vitro and in vivo study. The International journal of oral & maxillofacial implants 2001, 17, 793-798.
99. Wenz, H. J.; Bartsch, J.; Wolfart, S.; Kern, M. Osseointegration and clinical success of zirconia dental implants: a systematic review. The International journal of prosthodontics 2007, 21, 27-36.
100. Garvie, R.; Hannink, R.; Pascoe, R. Ceramic steel? Nature 1975, 258, 703-704.
101. Piconi, C.; Maccauro, G. Zirconia as a ceramic biomaterial. Biomaterials 1999, 20, 1-25.
102. Norowski, P. A.; Bumgardner, J. D. Biomaterial and antibiotic strategies for peri-implantitis: A review. Journal of Biomedical Materials Research Part B: Applied Biomaterials 2009, 88, 530-543.
103. Yildirim, M.; Fischer, H.; Marx, R.; Edelhoff, D. In vivo fracture resistance of implant-supported all-ceramic restorations. The Journal of prosthetic dentistry 2003, 90, 325-331.
104. Al-Ahmad, A.; Wiedmann-Al-Ahmad, M.; Fackler, A., et al. In vivo study of the initial bacterial adhesion on different implant materials. Archives of oral biology 2013, 58, 1139-1147.
105. Xu, K.; Liu, Y.; Liu, S., et al. Microorganism adhesion inhibited by silver doped Yttria-stabilized zirconia ceramics. Ceramics International 2011, 37, 2109-2115.
106. Cortizo, M. C.; Oberti, T. G.; Cortizo, M. S.; Cortizo, A. M.; Fernández Lorenzo de Mele, M. A. Chlorhexidine delivery system from titanium/polybenzyl acrylate coating: Evaluation of cytotoxicity and early bacterial adhesion. Journal of dentistry 2012, 40, 329-337.
107. Fürst, M. M.; Salvi, G. E.; Lang, N. P.; Persson, G. R. Bacterial colonization immediately after installation on oral titanium implants. Clinical oral implants research 2007, 18, 501-508.
108. Hauser-Gerspach, I.; Stübinger, S.; Meyer, J. Bactericidal effects of different laser systems on bacteria adhered to dental implant surfaces: an in vitro study comparing zirconia with titanium. Clinical oral implants research 2010, 21, 277-283.
109. Marsh, P. Microbial ecology of dental plaque and its significance in health and disease. Advances in dental research 1994, 8, 263-271.

110. Lima, E. M. C. X.; Koo, H.; Vacca Smith, A. M.; Rosalen, P. L.; Del Bel Cury, A. A. Adsorption of salivary and serum proteins, and bacterial adherence on titanium and zirconia ceramic surfaces. Clinical oral implants research 2008, 19, 780-785.
111. Mombelli, A. Microbiology and antimicrobial therapy of peri-implantitis. Periodontology 2000 2002, 28, 177-189.
112. Quirynen, M.; De Soete, M.; Van Steenberghe, D. Infectious risks for oral implants: a review of the literature. Clinical oral implants research 2002, 13, 1-19.
113. Badar, M.; Hemmen, K.; Nimtz, M., et al. Evaluation of madurahydroxylactone as a slow release antibacterial implant coating. The open biomedical engineering journal 2010, 4, 263.
114. Kälicke, T.; Schierholz, J.; Schlegel, U., et al. Effect on infection resistance of a local antiseptic and antibiotic coating on osteosynthesis implants: an in vitro and in vivo study. Journal of orthopaedic research 2006, 24, 1622-1640.
115. Ewald, A.; Glückermann, S. K.; Thull, R.; Gbureck, U. Antimicrobial titanium/silver PVD coatings on titanium. Biomedical engineering online 2006, 5, 22.
116. Petrini, P.; Arciola, C. R.; Pezzali, I., et al. Antibacterial activity of zinc modified titanium oxide surface. The International journal of artificial organs 2006, 29, 434-442.
117. Socransky, S. S.; Haffajee, A. D. Dental biofilms: difficult therapeutic targets. Periodontology 2000 2002, 28, 12-55.
118. Lu, Z. J.; Murray, K. S.; Vancleave, V.; Lavallie, E. R.; Stahl, M. L.; Mccoy, J. M. Expression of Thioredoxin Random Peptide Libraries on the Escherichia-Coli Cell-Surface as Functional Fusions to Flagellin - a System Designed for Exploring Protein-Protein Interactions. Nature biotechnology 1995, 13, 366-372.
119. Tamerler, C.; Khatayevich, D.; Gungormus, M., et al. Molecular biomimetics: GEPI-based biological routes to technology. Peptide Science 2010, 94, 78-94.
120. Tamerler, C.; Sarikaya, M. Molecular biomimetics: Utilizing naturels molecular ways in practical engineering. Acta Biomaterialia 2007, 3, 289-299.
121. Seker, U. O. S.; Wilson, B.; Dincer, S., et al. Adsorption behavior of linear and cyclic genetically engineered platinum binding peptides. Langmuir 2007, 23, 7895-7900.
122. Fjell, C. D.; Jenssen, H.; Cheung, W. A.; Hancock, R. E. W.; Cherkasov, A. Optimization of Antibacterial Peptides by Genetic Algorithms and Cheminformatics. Chemical Biology & Drug Design 2011, 77, 48-56.

123. Tamerler, C.; Oren, E. E.; Duman, M.; Venkatasubramanian, E.; Sarikaya, M. Adsorption kinetics of an engineered gold binding peptide by surface plasmon resonance spectroscopy and a quartz crystal microbalance. Langmuir 2006, 22, 7712-7718.
124. Hnilova, M.; Oren, E. E.; Seker, U. O. S., et al. Effect of Molecular Conformations on the Adsorption Behavior of Gold-Binding Peptides. Langmuir 2008, 24, 12440-12445.
125. Schirwitz, K.; Schmidt, A.; Lamzin, V. S. High-resolution structures of formate dehydrogenase from Candida boidinii. Protein Science 2007, 16, 1146-1156
126. Buck, R. P.; Lindner, E. Recommendations for Nomenclature of Ion-Selective Electrodes - (Iupac Recommendations 1994). Pure and Applied Chemistry 1994, 66, 2527-2536.
127. Enemchukwu, M.; Tafesse, F. Phosphate Sensitive Electrodes in Model Studies for Phosphorylation and Dephosphorylation Reactions. Analytical Letters 2013, 46, 663-670.
128. Kaur, H.; Garg, A.; Raghava, G. P. S. PEPstr: A de novo method for tertiary structure prediction of small bioactive peptides. Protein and Peptide Letters 2007, 14, 626-30.

7. Appendices

7.1 Appendix A

Primer sequences for *cm*FDH and *cm*FDH-AuBP2 construction:

To construct *cm*FDH-AuBP2 fusion protein, two double step PCR reactions were performed. In the first step PCR, pQE2-*cm*FDH template sequence was amplified for 15 cycles using forward primer 1 (5'-AGATCCATCAGGAGACAGTCCTACGGTCCTT GCGGTGGTGGTTCCATGAAGATCGTTTTAGTC-3'), and then the reaction was proceeded using the short forward primer-1 (5'- AGATCCATCAGGAGACAG -3') for an additional 30 cycles. Utilizing the resulting PCR product as the template, second step of PCR reaction was performed. In this step, the forward primer-2 (5'-TAGAGAGCTCAATGCGGCCCTTGGGCCCTGAGGAGATCCATCAGGAGACAG -3') and the short forward primer-2 (5'- TAGAGAGCTCAATGCGGCCCT -3') were used.

Primer sequences PreScission Protease Cleavage insertion:

In order to insert the PreScission Protease Cleavage site between the His-tag and the fusion protein, site-directed mutagenesis was applied to both constructs. For each of the *cm*FDH and *cm*FDH-AuBP2, one set of primer sequences, forward and reverse, were used. The forward and reverse primer sequences used for pQE2-*cm*FDH-AuBP2 are (5'-AGATCCATCAGGAGACAGTCCTACGGTCCTTGCGGTGGTGGTTCCATGAAGATCGTT TTAGTC-3') and (5'AGATCCATCAGGAGACAG-3), respectively. For pQE2-*cm*FDH, (5'TAGAGAGCTCAATGCGGCCCTTGGGCCCTGAGGAGATCC ATCAGGAGACAG3') and (5'TAGAGAGCTCAATGCGGCCCT 3') sequences were used as forward and reverse primers, respectively.

Recorded SPR sensograms of *cm*FDH and *cm*FDH-AuBP2 enzymes:

Binding kinetics of *cm*FDH and *cm*FDH-AuBP2 were analyzed using SPR spectroscopy. Figure A1 and A2 shows the recorded SPR sensograms of both *cm*FDH and *cm*FDH-AuBP2 enzymes at 0.25 and 0.5 µM concentrations.

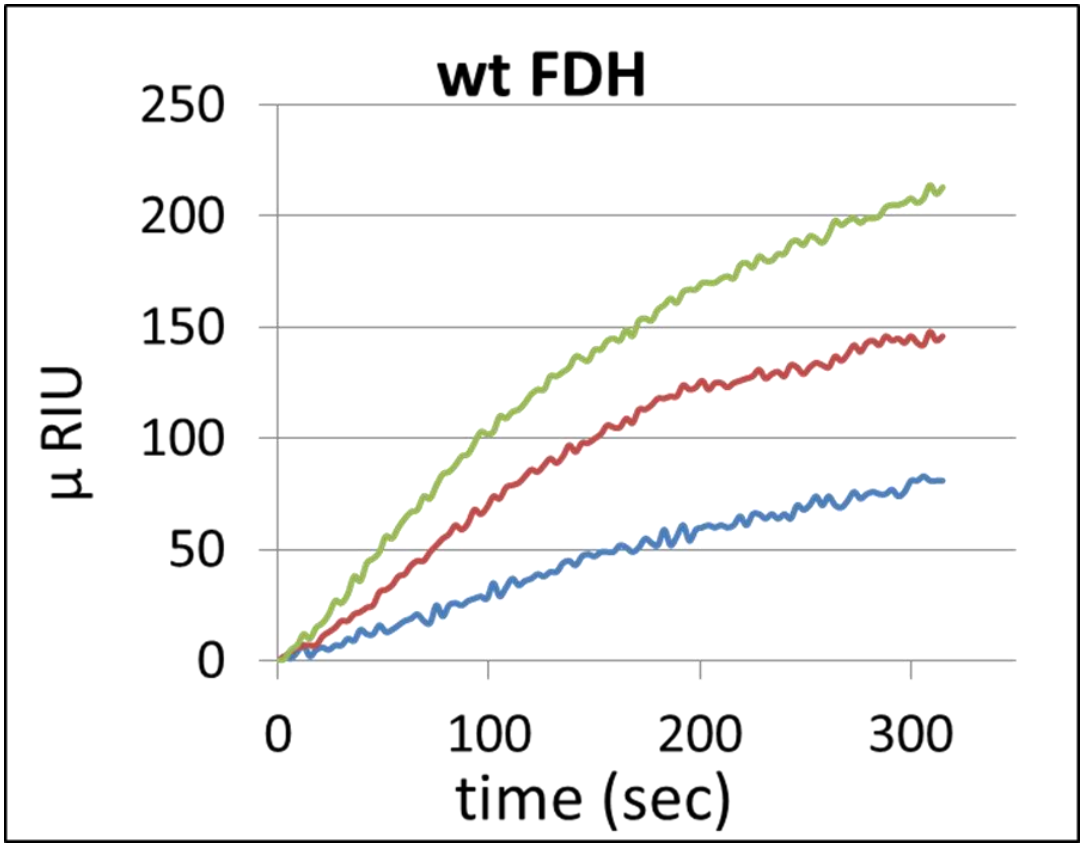

Figure A1. Adsorption kinetics of *cm*FDH at different concentrations.

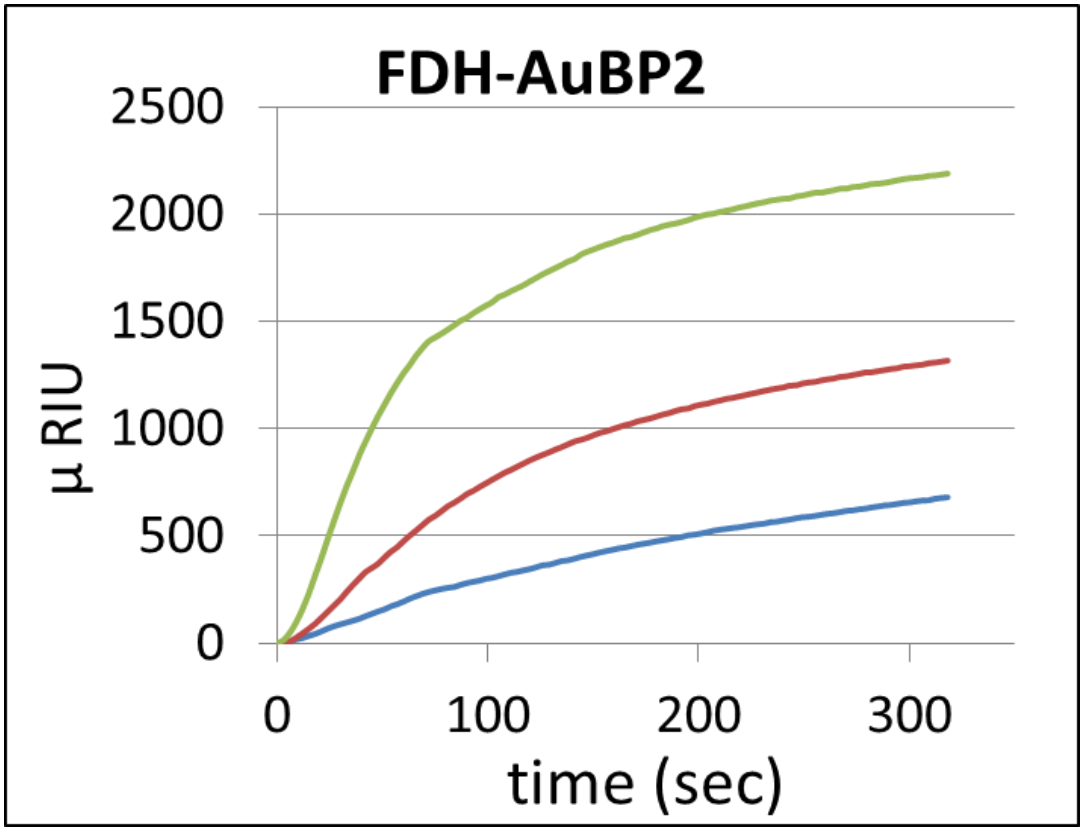

Figure A2. Adsorption kinetics of *cm*FDH-AuBP2 at different concentrations

7.2 Appendix B

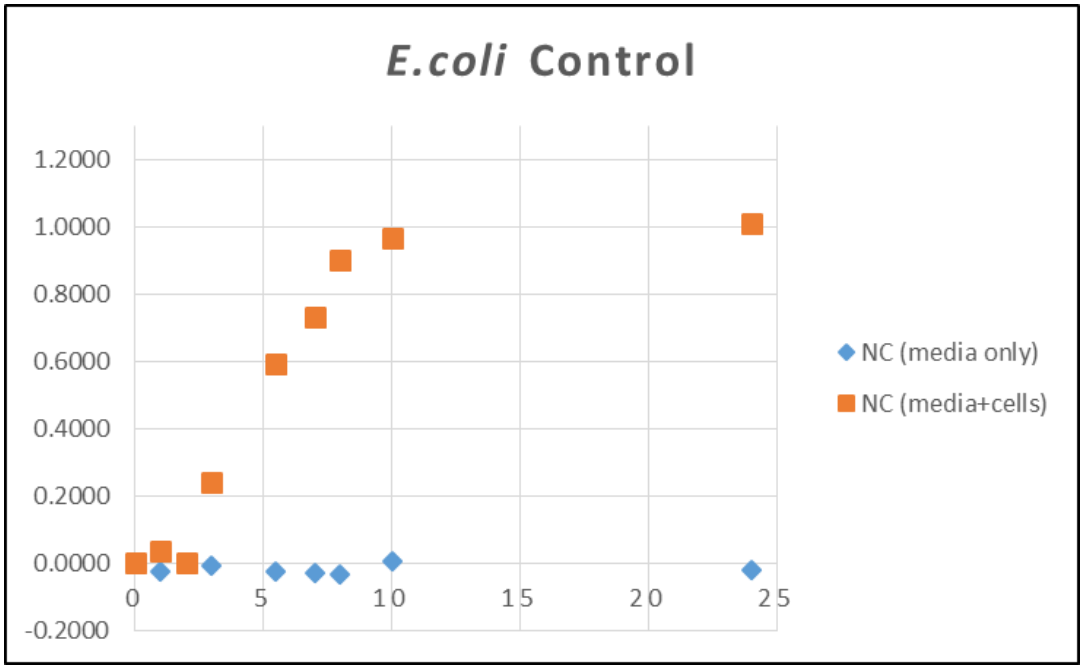

Figure B1. Growth of *E.coli* in the absence of AMP's.

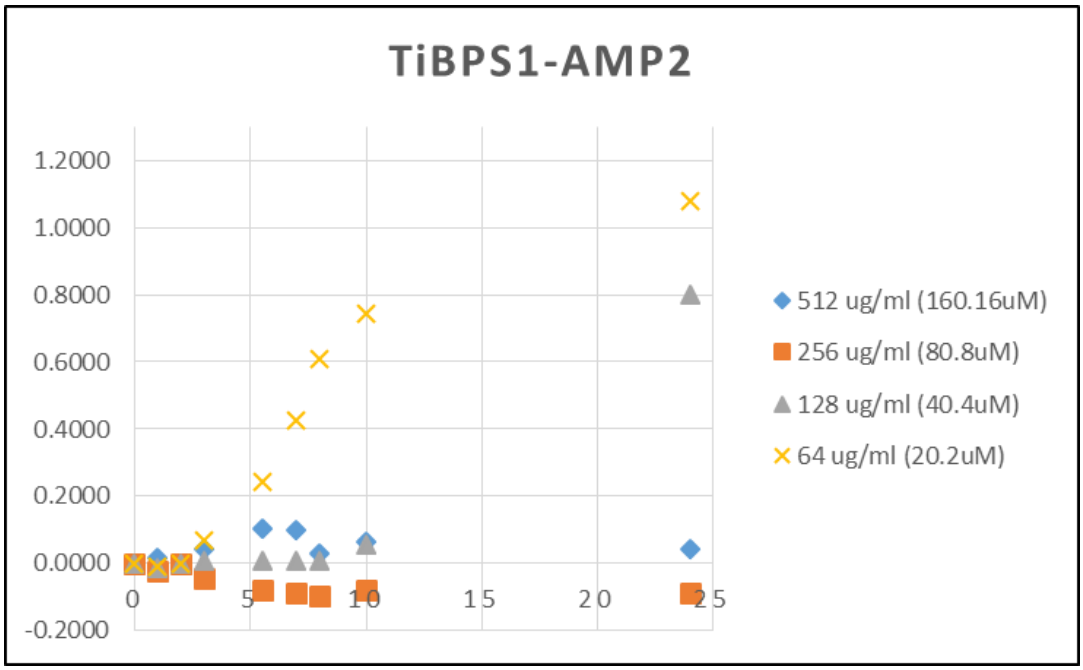

Figure B2. Growth of *E.coli* in the presence of TiBPS1-AMP2 peptide.

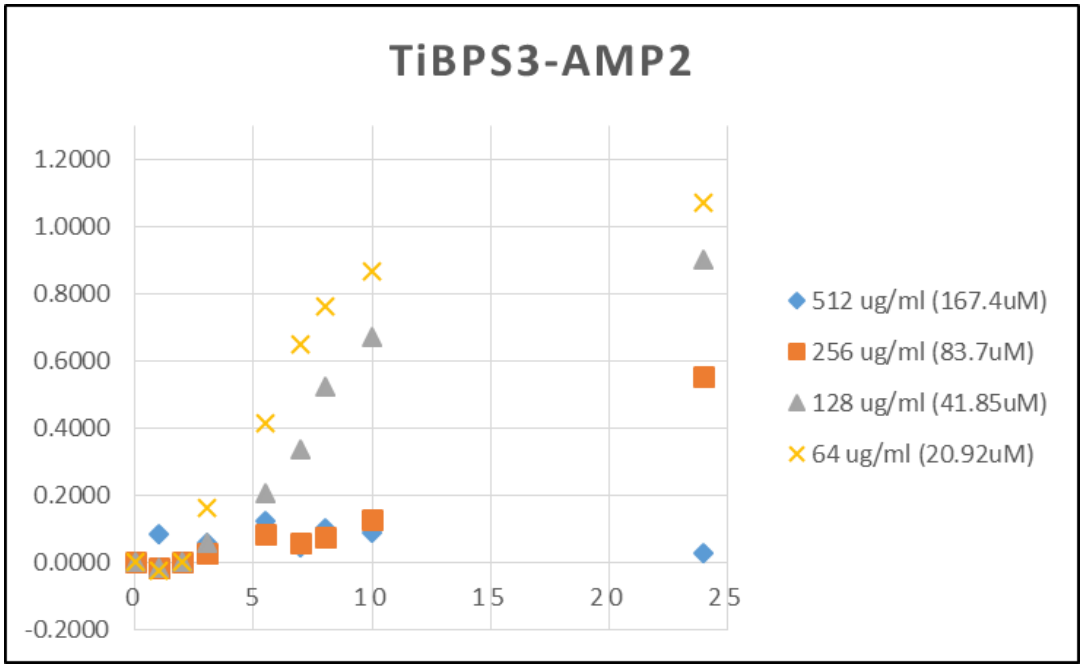

Figure B3 .Growth of *E.coli* in the presence of TiBPS3-AMP2 peptide.

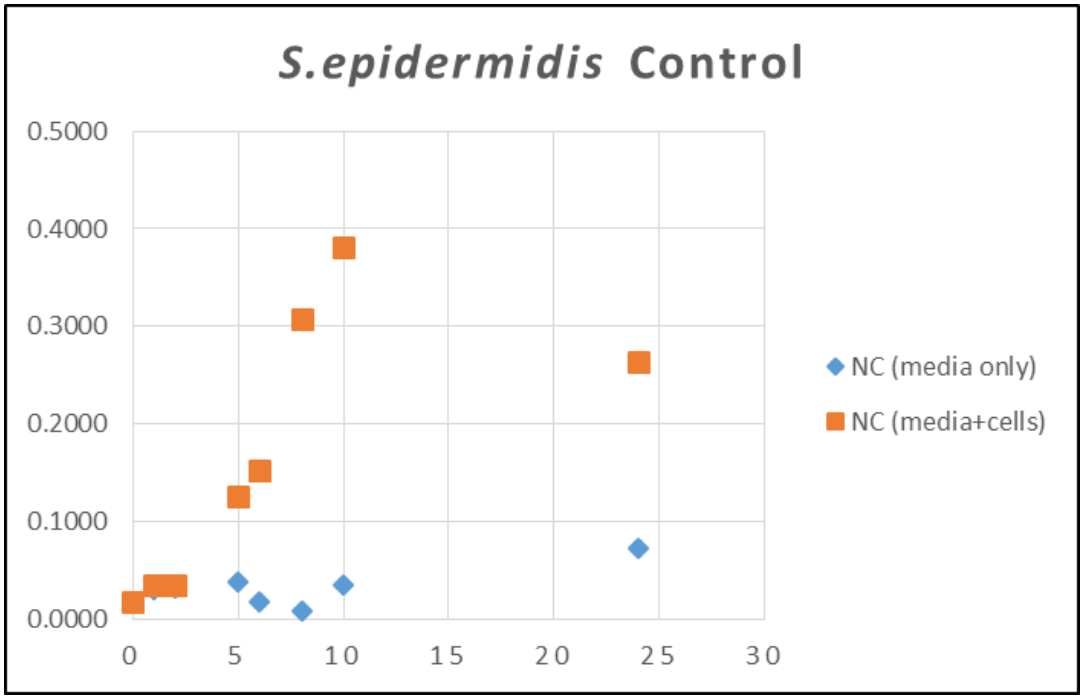

Figure B4. Growth of *S.epidermidis* in the absence of AMP's.

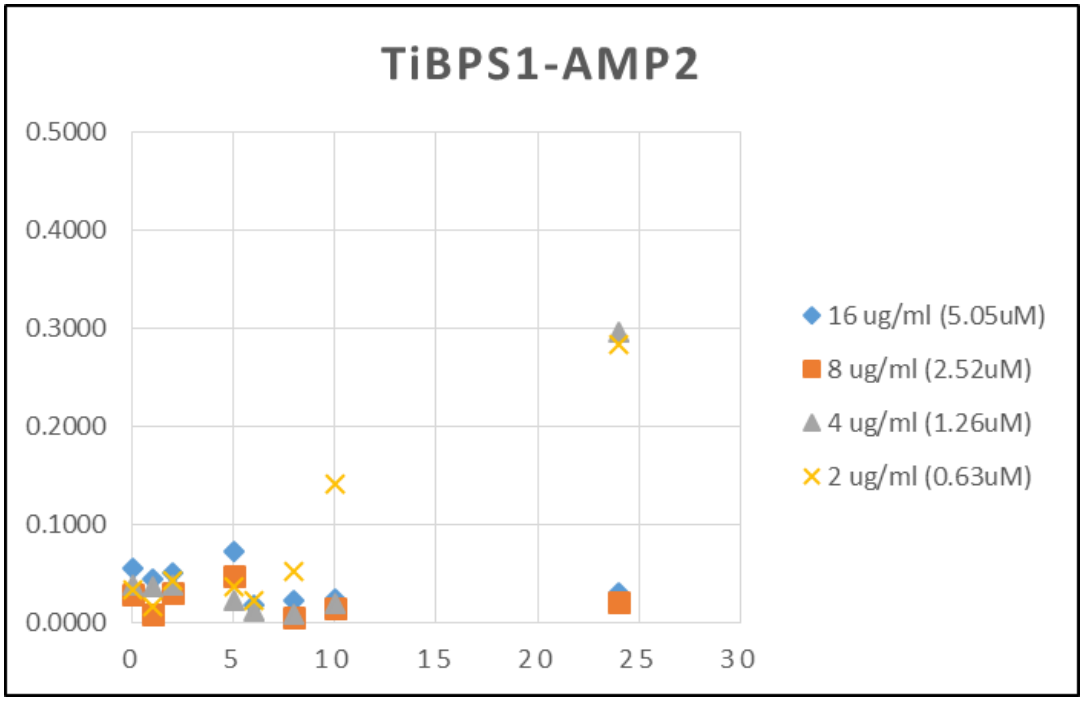

Figure B5. Growth of *S.epidermidis* in the presence of TiBPS1-AMP2.

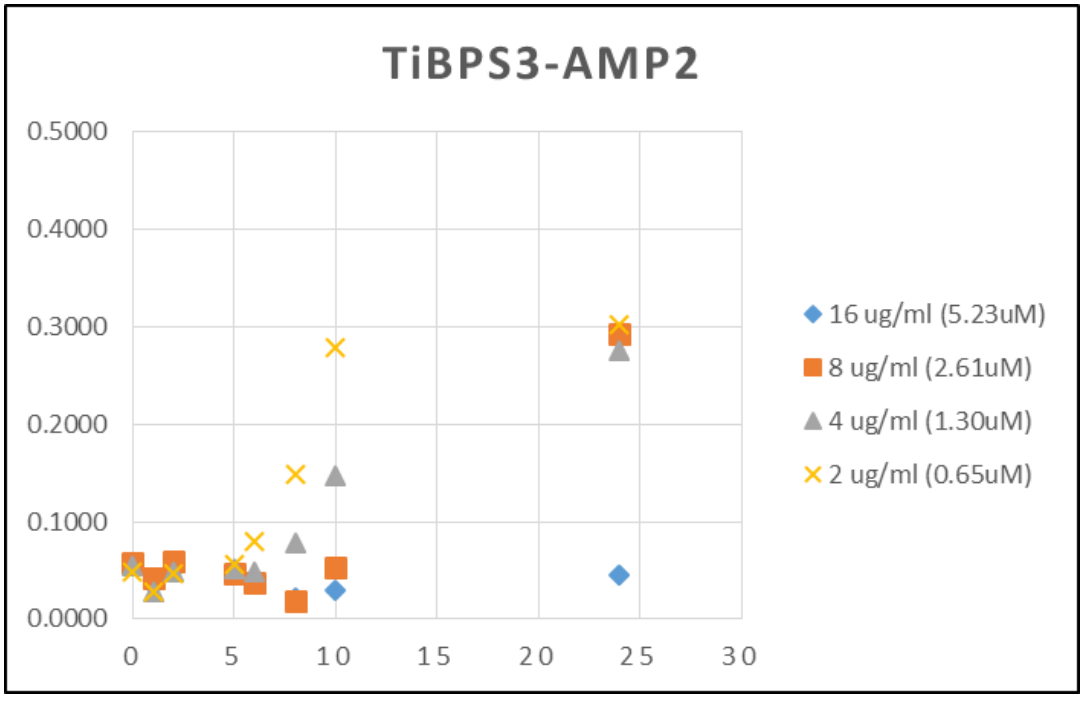

Figure B6. Growth of *S.epidermidis* in the presence of TiBPS3-AMP2.

7.3 Appendix C

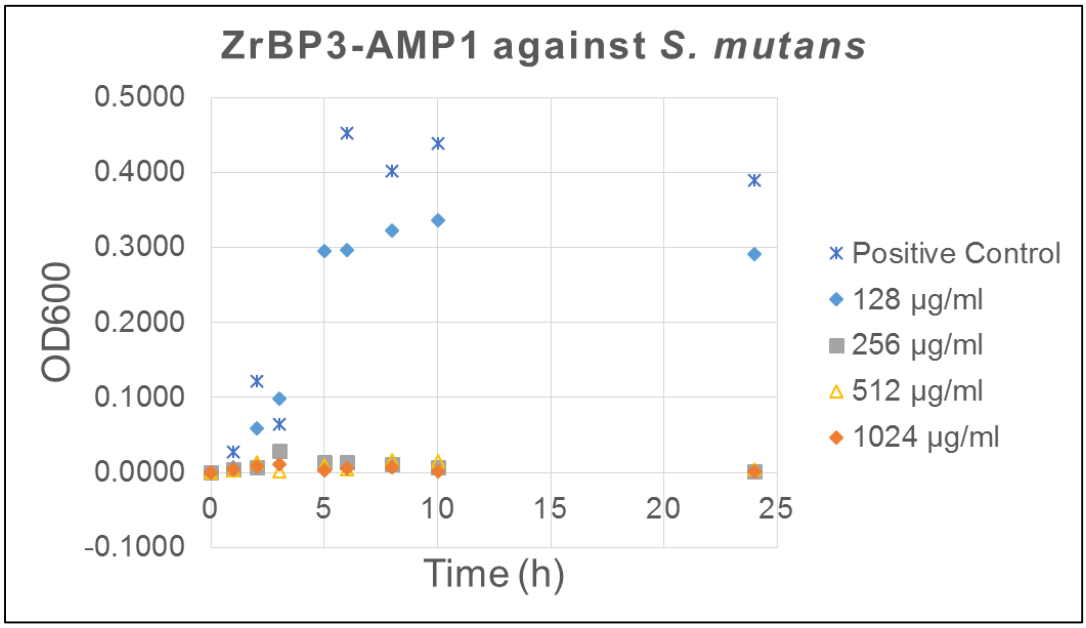

Figure C1. Growth of *S. mutans* in the presence of ZrBP3-AMP1 peptide.

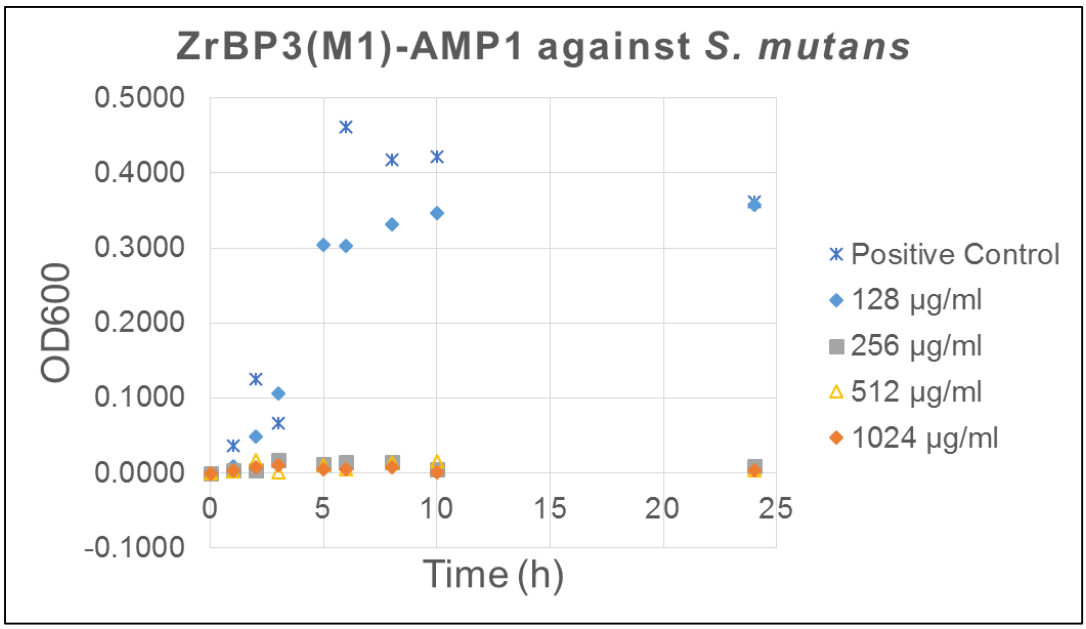

Figure C2. Growth of *S. mutans* in the presence of ZrBP3(M1)-AMP1 peptide.